Provided for non-commercial research and education use.
Not for reproduction, distribution or commercial use.

This article appeared in a journal published by Elsevier. The attached copy is furnished to the author for internal non-commercial research and education use, including for instruction at the authors institution and sharing with colleagues.

Other uses, including reproduction and distribution, or selling or licensing copies, or posting to personal, institutional or third party websites are prohibited.

In most cases authors are permitted to post their version of the article (e.g. in Word or Tex form) to their personal website or institutional repository. Authors requiring further information regarding Elsevier's archiving and manuscript policies are encouraged to visit:

http://www.elsevier.com/copyright

Author's personal copy

Deep-Sea Research I 55 (2008) 926–946

Contents lists available at ScienceDirect

Deep-Sea Research I

journal homepage: www.elsevier.com/locate/dsri

The outflow from Hudson Strait and its contribution to the Labrador Current

Fiammetta Straneo [a,*], François Saucier [b]

[a] Department of Physical Oceanography, Woods Hole Oceanographic Institution, MS 21, Woods Hole, MA 02543, USA
[b] Institut des Sciences de la mer, Université du Québec á Rimouski, 310 Allée des Ursulines, Rimouski, Que., Canada G5L 3A1

ARTICLE INFO

Article history:
Received 24 January 2007
Received in revised form
24 March 2008
Accepted 30 March 2008
Available online 12 April 2008

Keywords:
Hudson Strait
Hudson Bay
Labrador Current
Fresh water

ABSTRACT

This study describes the first year round observations of the outflow from Hudson Strait as obtained from a moored array deployed mid-strait from August 2004–2005, and from a high-resolution hydrographic section conducted in September 2005. The outflow has the structure of a buoyant boundary current spread across the sloping topography of its southern edge. The variability in the flow is dominated by the extreme semi-diurnal tides and by vigorous, mostly barotropic, fluctuations over several days. The fresh water export is seasonally concentrated between June and March with a peak in November–December, consistent with the seasonal riverine input and sea-ice melt. It is highly variable on weekly timescales because of synchronous salinity and velocity variations. The estimated volume and liquid fresh water transports during 2004–2005 are, respectively, of 1–1.2 Sv and 78–88 (28–29) mSv relative to a salinity of 34.8 (33). This implies that the Hudson Strait outflow accounts for approximately 15% of the volume and 50% of the fresh water transports of the Labrador Current. This larger than previously estimated contribution is partially due to the recycling, within the Hudson Bay System, of relatively fresh waters that flow into Hudson Strait, along its northern edge. It is speculated that the source of this inflow is the outflow from Davis Strait.

© 2008 Elsevier Ltd. All rights reserved.

1. Introduction

The Hudson Bay System (HBS) is a large, shallow, inland sea that includes Hudson, James and Ungava Bays, Foxe Basin and Hudson Strait (Fig. 1). It is characterized by a large riverine input (~900 km^3/yr; Déry et al., 2005) from an extensive drainage basin that covers much of the northeastern American continent. For comparison, the riverine input into the much larger Arctic Ocean (as defined by the Greenland–Scotland Ridge and Bering Strait) is only slightly more than three times larger (~3200 km^3/yr; Serreze et al., 2006). This sizable riverine input, combined with the inflow of waters of Arctic origin, via Fury and Hecla and Hudson Straits (Ingram and Prinsenberg, 1998), make the HBS an unusually fresh, large-scale arctic/subarctic estuarine system and the largest body of water in the world (area: ~million square kilometers) to completely freeze over in the winter and be ice-free in the late summer (Prinsenberg 1988).

Hudson Strait, a narrow (~100 km) and long (~400 km) channel with a mean depth of 300 m, is the principal opening of the HBS, connecting it to the Labrador Sea. Flow in the strait is in opposite directions along the two coasts: into the HBS along Baffin Island and out of the HBS along Quebec (Fig. 1; LeBlond et al., 1981; Drinkwater, 1988). This southeasterly flow, here termed the Hudson Strait *outflow*, combines with that from Davis Strait and with the retroflection of the West Greenland Current to form the Labrador Current (Mertz et al., 1993; Loder et al., 1998), a fresh-water-laden current that flows south along the Labrador coast. This current has a major impact on the shelf-slope waters of the entire North American coast

* Corresponding author. Tel.: +1 508 289 2914; fax: +1 508 457 2181.
E-mail address: fstraneo@whoi.edu (F. Straneo).

0967-0637/$ - see front matter © 2008 Elsevier Ltd. All rights reserved.
doi:10.1016/j.dsr.2008.03.012

Author's personal copy

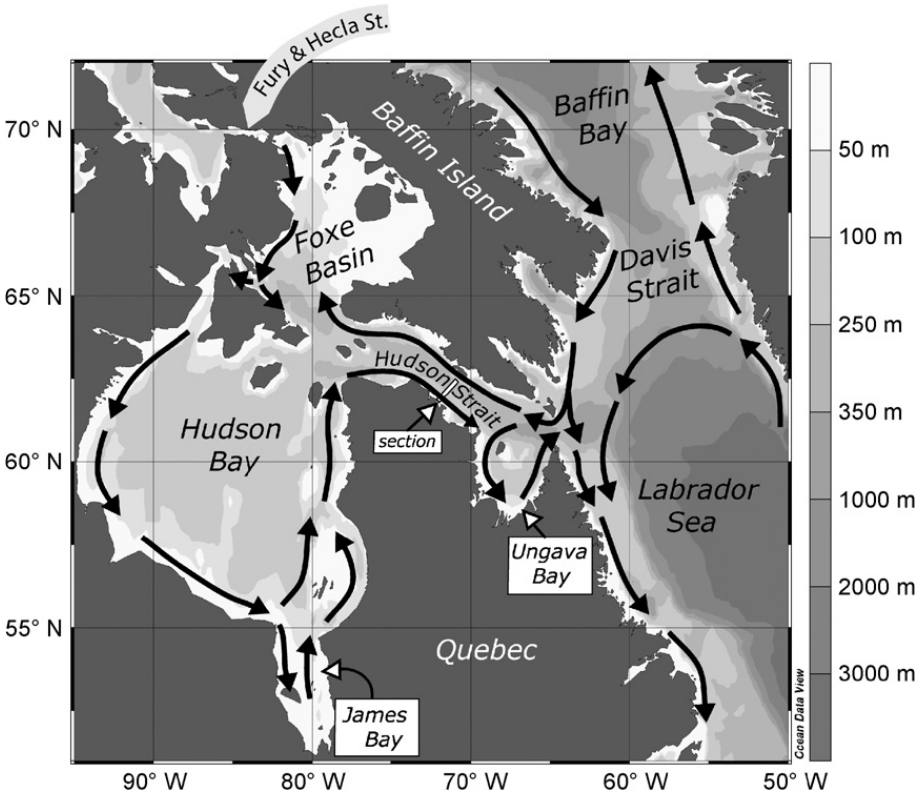

Fig. 1. Hudson Bay System: bathymetry and schematic circulation.

(Chapman and Beardsley, 1989) and the productive marine ecosystem and fisheries downstream (Loder et al., 1998). It also plays a significant role in the regional and basin scale climate of the subpolar North Atlantic due to its large fresh water content and its impact on stratification and associated water mass transformation processes. Indeed, the Labrador Current is thought to provide at least some of the fresh water that seasonally restratifies the deep convecting interior of the Labrador Sea and is an integral part of the convective seasonal cycle (Lazier et al., 2002; Straneo, 2006; Schmidt and Send, 2007).

The relative contribution of Hudson Strait to the structure, properties and variability of the Labrador Current is largely unknown, primarily because of the lack of data from the strait itself. Until recently, the only direct current measurements were from a four-mooring array deployed mid-strait, for a period of 2 months, in 1982. From these data, Drinkwater (1988) confirmed the existence of an inflow along the Baffin Island coast and an outflow along the Quebec coast, superimposed on the strong, mostly barotropic, tidal flows, but did not discuss the properties of the two currents. Later attempts to observe the flow through the strait for longer periods suffered from extensive instrument failure (Drinkwater, BIO/IMR, 2006, personal communication). Indeed, Hudson Strait's remote location, partial inaccessibility (due to the seasonal ice-cover) and challenging environment (extreme tides and drifting icebergs) have all contributed to its being under-observed.

Yet, there are many indications that the waters flowing out of Hudson Strait have a large impact on the Labrador Current and shelf downstream. For example, properties over the Labrador shelf differ markedly from those over the Baffin Bay shelf, further upstream, suggesting a strong influence from the Hudson Strait outflow (Lazier, 1982; Sutcliffe et al., 1983; Drinkwater and Jones, 1987). Similarly, the higher productivity of the Labrador shelf, relative to the Baffin Bay shelf, is largely attributed to the large nutrient input from Hudson Strait (Drinkwater and Harding, 2001). In terms of fresh water, the *net* fresh water transport (the difference between the outflow and the inflow) from Hudson Strait is estimated to be of the order of 42 mSv, which makes it the third largest net contributor of fresh water to the North Atlantic, after Fram and Davis Straits (at 160 and 72–130 mSv, respectively), relative to a salinity of 34.8 (Dickson et al., 2007). Given the estimated fresh water transport by the Labrador Current of 180 mSv, this tells us that approximately 1/4 of this fresh water originates from the riverine input into the HBS and the inflow via Fury and Hecla Strait.

Net contributions, however, cannot be equated to pathways and the fact that 1/4 of the fresh water of the Labrador Current *originates* from the net inputs into the HBS yields little information on the relative importance of Hudson Strait in feeding the Labrador Current. Investigating what fraction of the Labrador Current is due to the outflow from Hudson Strait is the focus of this study. This question is relevant to our understanding of what controls the seasonal and interannual variability of the Labrador Current and to the broader issue of how Arctic change will affect the circulation and ecosystems downstream (e.g., Greene and Pershing, 2007). Indeed, early attempts to attribute seasonal and interannual variations in salinity

Author's personal copy

over the Labrador shelf to variations in the river discharge into the HBS have yielded conflicting results (Prinsenberg et al., 1987; Sutcliffe et al., 1983; Myers et al., 1990). These discrepancies result from not knowing how the various fresh water inputs into the HBS are integrated into a variable fresh water export from Hudson Strait due to the systematic lack of data from the strait. Monitoring the outflow is even more relevant at a time when the river discharge has been decreasing (from 1964 to 2000; Déry et al., 2005).

In this study, we describe the first successful year round monitoring of the outflow by a three-mooring array deployed in August 2004 and recovered in September 2005. These measurements allow us to describe in detail the annual cycle and higher frequency variability of the outflowing current and its properties. In particular, we find that there is a discernible seasonal intensification of the fresh water and volume exports which is likely related to the strongly seasonal fresh water input by rivers and sea-ice melt. The bulk of the fresh water export during the fall occurs through a series of pulses of fresher waters associated with a speeding up of the flow. Superimposed on this lower frequency variability, we find that the along-strait subtidal currents are dominated by higher frequency (daily) barotropic fluctuations that are not linked with significant property variations.

From the moored data, the summer hydrographic data and historical current meter measurements, we are able to estimate the fresh water and volume transports into the Labrador Sea. These estimates confirm Hudson Strait's importance as a net contributor of fresh water to the North Atlantic and, furthermore, indicate that a large fraction of the fresh water carried by the Labrador Current (and a significant part of the volume) is due to the outflow from Hudson Strait. The larger than expected contribution is, in part, due to the recycling of fresh, inflowing waters along the northern edge of Hudson Strait whose properties, structure and timing are modified within the HBS. It is speculated that these inflowing waters are due to the Davis Strait outflow.

We begin by describing the circulation in the strait as observed from hydrographic data collected in the summer 2005. The mooring data are presented in Section 3, and their basic characteristics are described in Section 4. In Section 5, we analyze the dynamical structure of the outflow and argue that it is consistent with that of a buoyant gravity current over sloping topography. In the same section, we investigate the subtidal variability of the outflow field and its correlation with the observed variability in the density field and along-channel wind. The estimated volume, fresh water and heat transports out of the strait are presented in Section 6.

2. Hydrography

The dominant features of the two-way circulation in the strait are evident in the hydrographic data shown in Fig. 2, collected over 2 days in September 2005. The southernmost station is 1 km from Wales Island which, in turn, is separated from the coast of Quebec by a shallow (<20 m) and narrow (<2 km) sound. The northernmost station, similarly, was less than 2 km away from Big Island, separated from Baffin Island by a narrow, shallow passage. Thus, for all purposes the section is representative of the flow across the entire strait (see Fig. 1 for section location).

The section shows a wedge of fresh water that extends from the coast of Quebec approximately 40 km offshore (Fig. 2a), consistent with Drinkwater's (1988) description of a current along the southern shore that carries the fresh waters into the Labrador Sea. Beneath the outflowing fresh water, a saltier and cold (at freezing point) water mass is located above the 100–150 m isobath (Fig. 2b). Since density is controlled by salinity at these temperatures, it is the water mass' salt content that determines its position in the water column. Isopycnals flatten over the central portion of the strait whose central waters are relatively saltier than those found at the same depth on either side of the strait. On the northern side, the isopycnal slope is consistent with the inflow of relatively warm and salty waters ($S\sim33$, $-0.5\,^{\circ}\mathrm{C}<T<1\,^{\circ}\mathrm{C}$; Fig. 2a and b) along the coast of Baffin Island. A relatively thin warm layer due to summer heating is found at the surface across the entire section.

The different characteristics of the outflow and inflow are particularly striking if one considers the vertical stratification (Fig. 2c). On the southern side, waters are strongly stratified for densities above 26.4 (salinities lower than 32.9–33) and more weakly stratified beneath. On the northern side, the water column is very weakly stratified throughout. This is consistent with the strong mixing (especially due to tides) that occurs at the mouth of the strait (LeBlond et al., 1981). At depth, the mid-strait waters are characterized by thick bottom boundary layers, likely a result of the strong barotropic tidal flows in the strait and a relatively long residence time of these water masses (Drinkwater, 1988; see also Fig. 6 in Saucier et al., 2004). The geostrophic, along-strait velocity, derived by assuming zero velocity at the bottom, shows the different character of the outflow and inflow (Fig. 2d). The former is a strongly baroclinic, surface-intensified current while the latter is mostly barotropic. Both currents appear to be confined within 40 km of the coast, which coincides, roughly, to the width of the sloping topography along the strait.[1] We note that because the section was occupied over a period of 2 days and given the large variability observed in the outflow, this section is only quasi-synoptic.

One characteristic of the waters of the HBS is a marked property difference between waters that are influenced by the fresh water input from rivers and sea-ice melt and the deep/intermediate waters that are not (Jones and Anderson, 1994; Ingram and Prinsenberg, 1998). We see this in the salinity versus depth and T/S properties of the central and outflowing strait waters (Fig. 3a and b). Notice, in particular, the large vertical stratification and freshness of the waters that are lighter than $\sigma_t\sim26.4$ (or equivalently with salinities lower than 33) compared to the weak

[1] The topographic slope at Big Island (essentially a vertical wall) is not representative of the mean slope along the coast of Baffin Island.

Author's personal copy

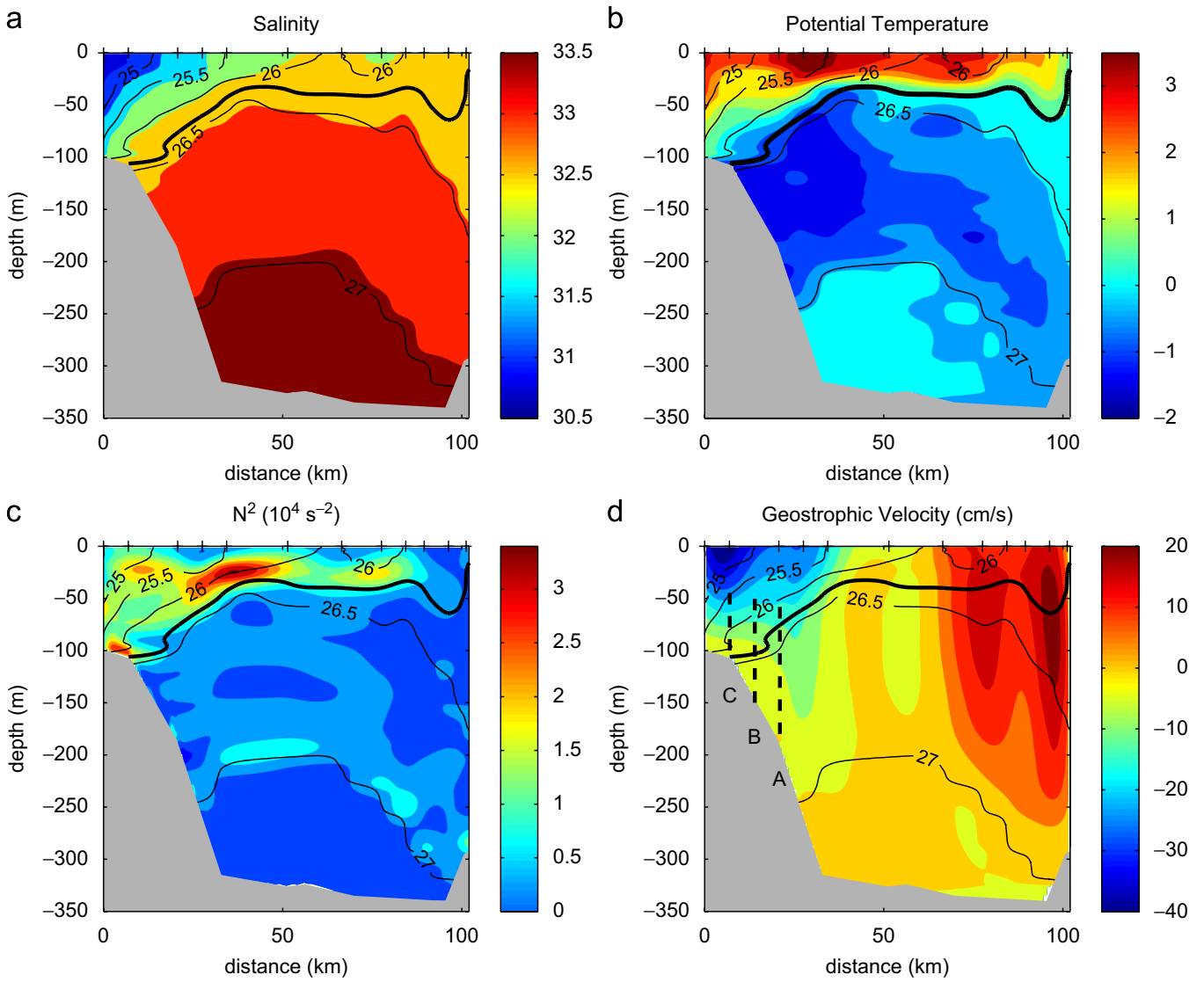

Fig. 2. (a) Salinity, (b) potential temperature (°C), (c) Brunt–Vaisala frequency squared, and (d) geostrophic velocity, from a hydrographic survey across the strait in September 2005. Isopycnals are overlaid on all panels, with the $\sigma_t = 26.4$ in bold. Station location is indicated at the top of each plot. The three mooring locations are shown in (d).

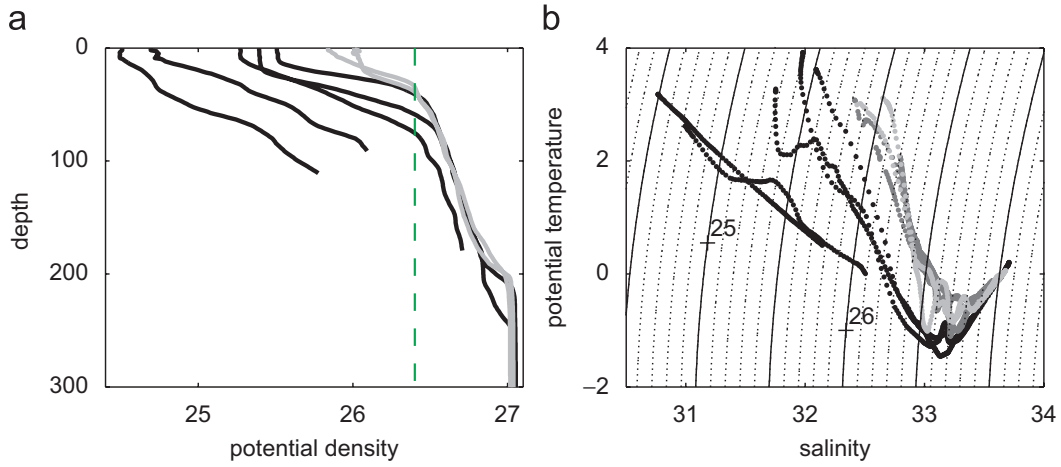

Fig. 3. (a) Density profiles from hydrographic data for stations in the outflow (black lines) and center of strait (gray). Vertical dashed line indicates the 26.4 potential density line. (b) *T*/*S* properties for all stations shown in Fig. 2 section divided into outflow (black), center (dark gray) and inflow (light gray). We define the outflow/inflow as those within 40 km of the respective coast, and the center stations are those offshore of 40 km.

Author's personal copy

vertical stratification of the denser, saltier waters. This distinction is evident even if the separation occurs at different depths across the section (Fig. 2c). As expected, this characteristic is not found in the inflowing waters along the northern shore, which are characterized by a weak stratification throughout (Fig. 3b). Finally, from the T/S properties one can infer an approximate width of 40 km for both the outflowing and inflowing current; offshore of this distance the water properties over the central portion of the strait are characterized by distinct properties and intrusions from both sides (Fig. 3b).

3. Mooring data

The moorings occupied a section, approximately mid-strait (Fig. 1), that was chosen for both scientific and practical reasons. The mouth of the Strait is characterized by strong, turbulent flows and persistent eddies, due to the interaction of the strong tidal flow with the numerous channels and islands (LeBlond et al., 1981), which would make it difficult to extract the mean flow and secure moorings. Also the region between the section occupied and the mouth of the strait is characterized by a strong recirculation that would render distinguishing the through-flow from the recirculating portion arduous. This same recirculation poses a practical threat to the moorings since it carries numerous icebergs (Drinkwater, 1986). The section chosen is far enough from the mouth of the strait to avoid the bulk of the recirculation and the drifting icebergs. Finally, this section is slightly west of the one occupied by the 1982 array described by Drinkwater (1988) but coincides with that of the array deployed in 1986, which suffered widespread instrument failure (Drinkwater, BIO/IMR, 2004, personal communication).

3.1. Instrumentation

Three moorings, A, B and C, were deployed across the sloping topography on the southern side of the Strait, C being the most onshore one (Fig. 2d). The depth of the water at the sites is 180, 150 and 100 m, respectively. The upper instrument at the three moorings was at 55, 35 and 40 m, respectively, to avoid collisions with icebergs and sea-ice ridges. Moorings B and C were similar in design, each carrying a 300 kHz upward looking Acoustic Doppler Current Profiler (ADCP) (respectively, at 135 and 93 m) that recorded velocity every half hour in 4 m bins, and two Seabird SBE37 Microcats on each (35/55 at B and 40/60 at C) that recorded temperature, salinity and pressure every 30 min. A string of temperature loggers (roughly one every 10 m sampling every 30 min) was also present on both B and C. Data return for B and C was 100%. Mooring A was more heavily instrumented than B and C. It carried a McLane Moored Profiler (MMP), a 75 kHz long-range ADCP, a Seabird SBE37 Microcat at 170 m, an Arctic Winch mounted on the top flotation sphere (providing daily temperature and salinity profiles between the surface and 60 m) and an Upward Looking Sonar (ULS) to measure pressure, tilt and sea-ice draft. The MMP was scheduled to profile every 2 h between 60 and 170 m logging temperature and salinity; the time taken to profile the 110 m was roughly 10 min. It functioned correctly until 7 March, when it suffered a hardware problem. Thereafter, until it was recovered, it slowly moved up and down the water column at an irregular rate (see Fig. 5). The long-range ADCP was programmed to measure velocity over the entire 170 m water column in 10 m bins and at a 15-min sampling rate. Unfortunately, it stopped recording after 21 days because of an electrical failure. The Microcat at 170 m recorded temperature and salinity every 5 min for the entire year. Finally, the ULS did not record sea-ice draft because of a hardware problem.

The Arctic Winch is a new instrument designed to address a common problem of moorings: making measurements close to the surface (where, for example, the freshwater resides) while not leaving any permanent part of the mooring exposed to its adverse conditions: drifting sea-ice, icebergs, ship traffic and surface waves. It consists of two elements: a float and an electrical winch. The float, carrying the sensors, is connected to the winch via a non-conducting cable (to minimize weight and drag) and docks in a basket on the mooring's top float. Periodic unspooling of the cable allows the buoyant float to collect a profile. The float is retrieved whenever there is a reduction in tension of the cable (because it is at the surface or has hit an obstacle such as ice) or when a maximum length of cable has been paid out. It carries a Falmouth Scientific Inc. CTD (Conductivity, Temperature, Depth recorder). While it did profile once a day for the year, after the first month the float progressively failed to reach the surface, eventually reducing its profiling range from 60 m to about 5 m. Post-recovery inspection revealed that a small sea-water leak into the winch had shorted its windings, effectively acting as a break. Beyond the profiles, the winch provides a daily record of temperature and salinity at the top of A (58 m).

3.2. Data calibration and processing

The CTDs on the moorings were all calibrated prior to deployment. Post-recovery calibration, to account for any drift, was carried out using hydrographic casts collected just prior to recovery or by checking drift by comparing to nearby instruments. Two conductivity sensors appeared to have drifted slightly, and the salinity records were corrected by assuming a linear drift.

The ADCP data were quality controlled by removing all data points with error velocities larger than 0.2 m/s; overall this amounted to less than 2% of data at all moorings. These data gaps were filled by interpolating in the vertical. Approximately, 8% of the data were lost to side lobe interference which resulted in no data over the upper 20 m at A and 12 m at B and C. The depth of the transducer was obtained by deriving a corrected sound speed, at the transducer depth, from the Microcat data at the ADCP depth, at A, and from the Microcat data at 60 m at B and C. The same correction was used to derive the depth array for the bins. Directions from the ADCPs were corrected for magnetic declinations of 29.6, 29.35 and 29.23 W at A, B and C, respectively.

Author's personal copy

The strong tidal currents in the strait caused moorings B and C to blow down several meters during strong flows and as much as 10 m in a handful of cases. Gaps in the instrument records at B and C, due to blow down, were filled via linear interpolation in time. Mooring A, on the other hand, was designed to be particularly stiff, and the pressure record on the ULS reveals that the top float (a sphere with a buoyancy of 2000 lb.) was not blown down more than 2.5 m. The tidal range at A exceeded 8 m.

4. Overview of the properties of the outflow

4.1. Salinity and temperature

The properties of the upper layers in the outflow are characterized by a large annual variability. The freshest waters are observed from June to March with peak fresh periods from mid-October to mid-December at all three moorings (Figs. 4 and 5). The variability in salinity across the array is much less than the seasonal variability. During the fresh period, we observe large salinity fluctuations over periods of several days to weeks which are highly coherent throughout the array in both the across-strait direction and in depth. During the remainder of the year (mid-March–June), the variability is greatly reduced and higher salinity waters flow past the moorings. A minimum salinity of 28.8 was observed at the 40 m Microcat at C while a maximum salinity of 33.58 was observed at A at 170 m. In general, salinity increases offshore and with depth. The seasonality at depth, as observed at mooring A, is greatly reduced. We note that the seasonal freshening is consistent with the strongly seasonal riverine input (Déry et al., 2005) and sea-ice melt (Prinsenberg, 1988). At the same time, how long the fresh water resides in the upper layers of Hudson Bay is still an open question (Déry et al., 2005).

Temperature exhibits a different seasonality from salinity. Waters are at or close to the freezing point O($-1.8\,^{\circ}$C) for the greater part of the year (from December to July), and the temporal variability is relatively small (Figs. 4 and 5). Warming of the surface layers starts in July and peaks in mid-September. At depth, this seasonal warming is observed with a delay: the warmest waters at 170 m occur 2 months later than at 55 m (Fig. 5). This is consistent with a downward mixing of heat and advection by a sheared, mean flow. Similarly to salinity, temperature fluctuations are strongly coherent across the array.

More quantitatively the horizontal correlation for both temperature and salinity is significant between all moorings: $r>0.9$ at 40 and 60 m between B and C and $r\sim0.9$ between B and A at 60 m. In the vertical, correlations between 40 and 60 m are very high ($r>0.95$) both at B and at C. At A, where we have data from 60 to 150 m, the correlation between the salinity and temperature observed at 58 m and other depths is always significant at the 95% confidence level even if decreasing with depth, $r>0.7$ (0.6) for salinity (temperature) between the uppermost and deepest measurements. These results are consistent with a strongly mixed and stirred environment, likely due to the large tidal forcing in Hudson Strait.

4.2. Velocity

The mean annual flow observed at B and C is mostly along-strait (125°N true) and directed towards the

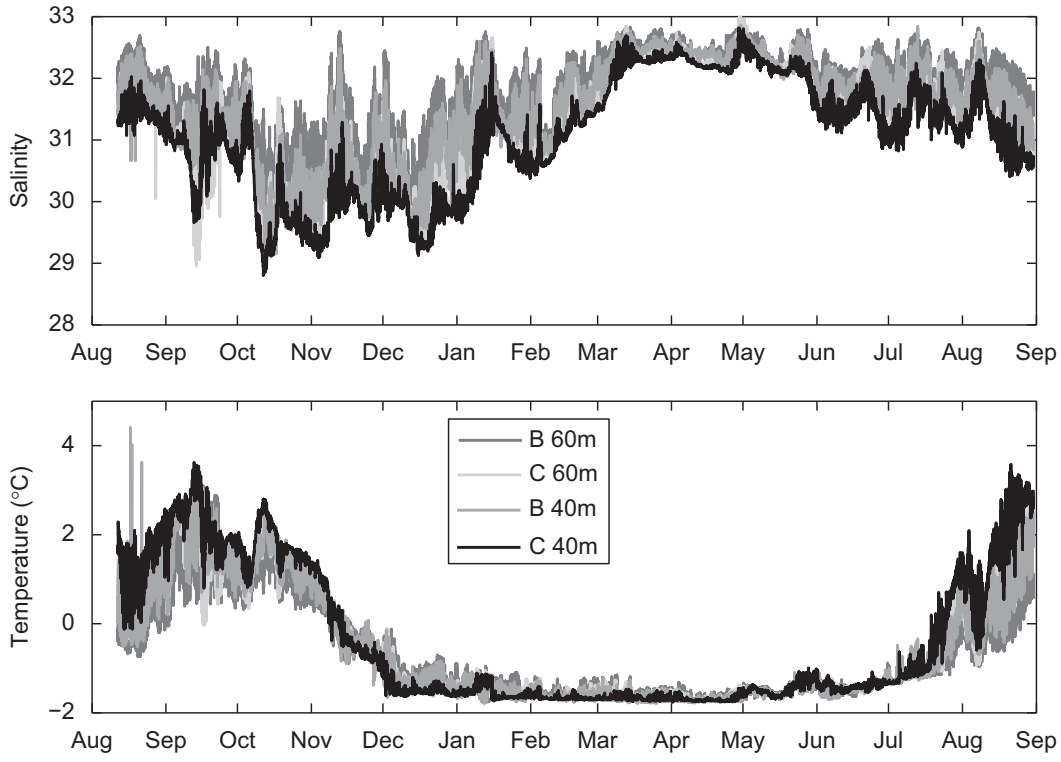

Fig. 4. Salinity and temperature from the Microcats on moorings B and C.

Author's personal copy

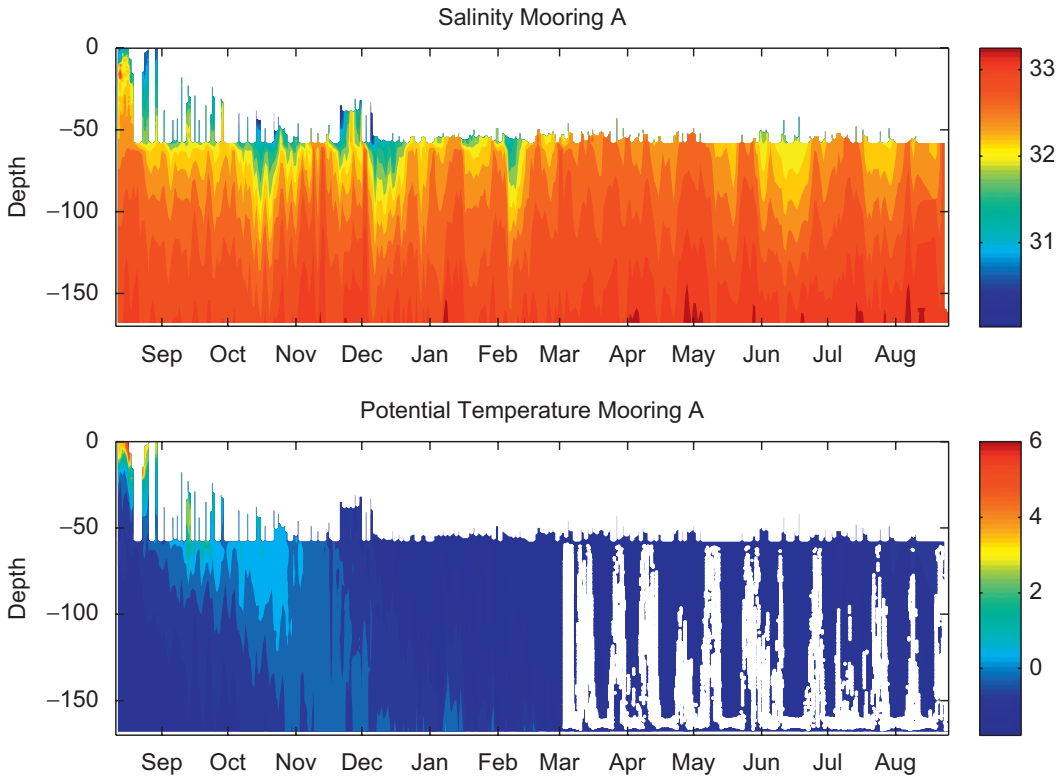

Fig. 5. Composite salinity and potential temperature at A using data from all instruments. The data were gridded and interpolated as described in Appendix A. The tracks of the MMP after the mechanical failure are overlaid in white on the temperature plot only.

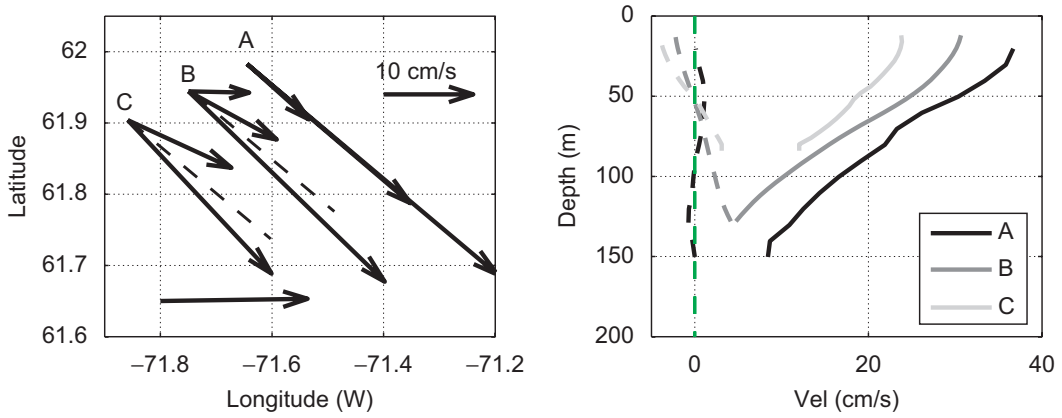

Fig. 6. Left: mean annual flow at the three moorings at the following depths: C (40, 80), B (40, 80, 120), and A (40, 80, 150 m); amplitude decreases with depth. At A the mean is for the 21 days of ADCP data. The thin black line overlaid at each mooring location shows the strait's orientation (125°N true). The arrow labeled *wind* shows the annually averaged wind direction from August 2004 to August 2005 from the operational analyses (NOWCAST) and 12-h forecast cycles issued from the Canadian Meteorological Center using the Global Environmental Multiscale Model (GEM). Right: mean vertical structure of the along-strait (solid) and across-strait (dashed) flow at the three moorings.

Labrador Sea (Fig. 6). The same is true for the average flow observed at A during the 21 days while the ADCP was working. (The fact that at B and C the annually averaged velocities were not very different from those observed during the first 21 days suggests that the mean at A, observed during the first 21 days, is likely similar to the mean annual flow.) The mean along-strait currents decrease linearly with depth at all three moorings even if the speed 20 m off the bottom, at B and C, is still significantly different from zero. The counterclockwise veering with depth, at B and C, implies a net onshore flow at the surface and offshore at depth. This is consistent with a net downwelling along the Quebec shore driven by the predominantly westerly (from the west) winds over the region (Fig. 6).

The annual mean, however, is deceivingly simple given the strong variability on a variety of time scales observed in the strait (Fig. 7). Peak flows exceed 1 m/s in the along-strait direction with a tidal current amplitude of comparable magnitude. The tidal variability is dominated by the semi-diurnal tide (M2 followed by S2), which accounts for almost 70% of the total variance (compared to only about

Author's personal copy

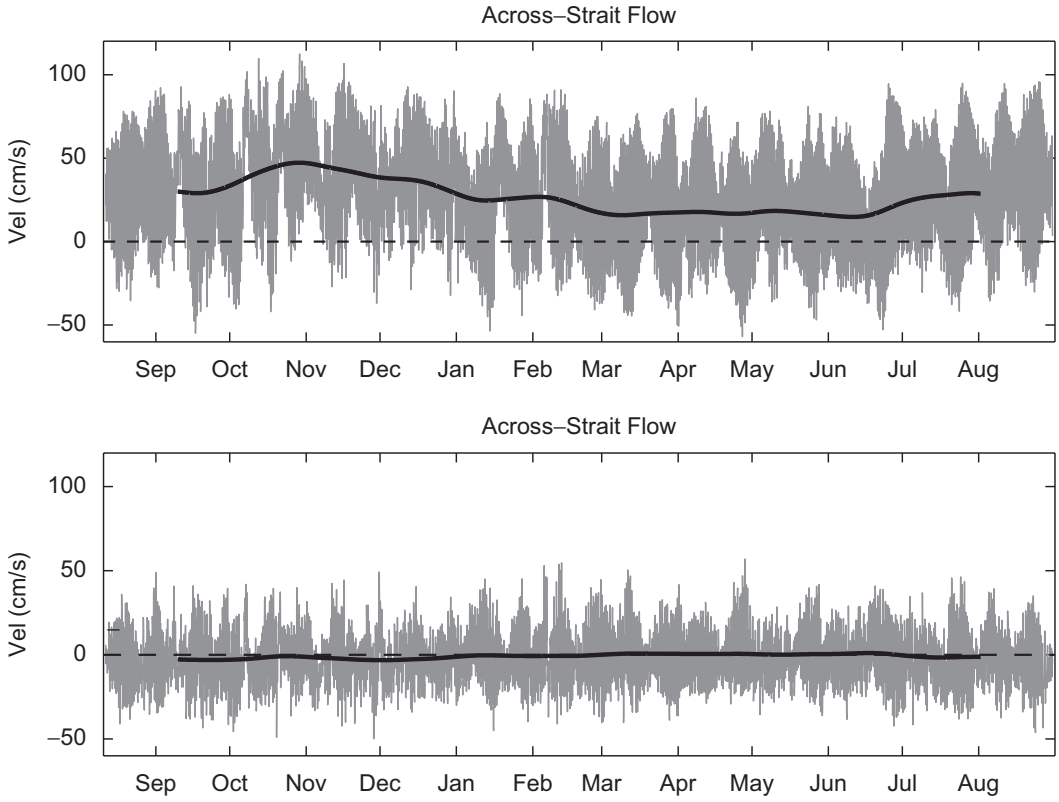

Fig. 7. Along- and across-strait flow at 40 m at B. Two-month low-pass filtered time series is overlaid in bold.

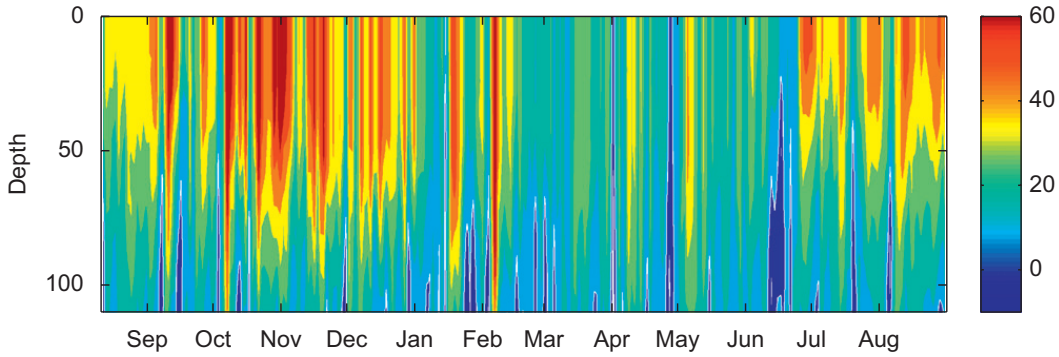

Fig. 8. Along-strait flow at B (in cm/s) as a function of depth. The tidal variability was removed using a 34-h four-point Butterworth filter. The white contour is the zero velocity.

6% for the diurnal). The tidal currents are predominantly barotropic and mostly aligned along-strait, in agreement with the description of the tidal currents given in Drinkwater (1988) from the 1982 array. An in-depth analysis of the tidal currents in the Strait is ongoing and will be presented in a separate publication. The across-strait flow is dominated by tides, albeit with a reduced amplitude, and there is no significant mean flow (or seasonality) at this depth (40 m). The velocity records at B and C, and, where data exists, at A are significantly correlated even after the tides are removed. Horizontal correlations vary with depth but are typically above 0.6.

Once the tidal variability is removed (using a 34-h four-point Butterworth filter), we observe large velocity variations on timescales of the order of a few days (Fig. 8). Bursts of flow towards the Labrador Sea alternate with a weakening of the outflow over the entire water column with frequent reversals at depth. During the period when the outflow waters are weakly stratified (between March and June), these reversals can, at times, extend to the surface. On longer timescales, the 2-month low-pass filtered along-strait velocity (Fig. 7) shows a weak seasonal cycle with maximum outflow in November and minimum outflow from March to June, which coincides with the passage of the fresh water.

5. Dynamical characteristics of the outflow

After the basic description of the outflow's properties and velocity given above, we investigate the extent to which the structure of the outflow and its variability are

Author's personal copy

consistent with some basic dynamical balances. Specifically, we are interested in determining if the outflow has some stable characteristics that may, in turn, be indicative of the dynamical processes that are shaping it.

5.1. Stability of the vertical density structure

First, we examine the extent to which the features observed in the synoptic hydrographic section (Figs. 2 and 3) apply to the data collected throughout the year. In particular, in Section 2 we argued that the outflowing waters could be separated into two basic classes: the fresh waters that are affected by the seasonal fresh water input into the HBS and the deeper waters that lay beneath these. From the hydrographic data, we found that these are generally distinguishable by their stratification (the fresh waters are highly stratified) and their density (the fresh waters are lighter than $\sigma_t = 26.4$). Here, we use the over 2400 profiles of temperature and salinity, between 60 and 170 m, collected by the moored profiler, to investigate the extent to which these characteristics are stable in time.

One way of doing this is to re-arrange the profiles based on the salinity observed at a given, fixed depth (Fig. 9a). If the relationship between stratification and density is independent of depth, then we expect profiles with similar densities at a given depth to look similar. The fact that the isopycnal contours are mostly parallel when thus re-arranged signifies that the layer thickness between two isopycnals is mostly invariant (i.e., the stratification associated with a given density is mostly constant). Such a characteristic can be used to infer a mean density profile for the outflow by estimating the mean thickness, associated with defined isopycnal pairs, and use it construct a representative density profile versus an arbitrary depth axis (Fig. 9b). The individual profiles are also shown in Fig. 9b by shifting them in depth so that the actual profile and the reconstructed profile intersect at the top of the profile (60 m). From this analysis, we can conclude that, as was observed in the summer hydrographic data, the fresh layers of the outflow are strongly (and uniformly) stratified and tend to be lighter than 26.4, in contrast with the more weakly stratified deeper waters. Also, these results suggest that the fresh waters undergo mixing, which distributes the fresh water over a relatively thick layer while maintaining a large vertical stratification.

5.2. Geostrophy and basic dynamic balance

Given the observed velocities and the limited variations in topography along the strait, we expect the flow to be in semi-geostrophic balance in the along-strait direction. To verify this, we evaluate the validity of the thermal wind balance relation as follows. We calculate the horizontal density gradient at 60 m at the central mooring, B, by using the 60 m salinity and temperature records from the two neighboring moorings (A and C). The vertical shear in the along-strait flow at B at 60 m is calculated by using the velocities at 40 and at 80 m from the ADCP data at B. The time series for the two sides of the thermal wind equation are shown in Fig. 10. Overall there is good agreement in both magnitude and phase, and the two fields are significantly correlated ($r = 0.76$, with maximum correlation at zero lag). We note that this method is likely to underestimate the extent to which the flow is in semi-geostrophic balance since it assumes that the horizontal density gradient across the entire width of the array (14 km) is representative of the local horizontal density gradient at B.

Beyond semi-geostrophic balance, the outflow from Hudson Strait has the typical characteristics of a buoyant coastal current over sloping topography. These currents tend to be wider than the deformation radius (the expected width of a buoyant current flowing along a vertical wall) because of the lateral spreading induced by bottom friction. Their structure (width, height, isopycnal slope) reflects a balance between the frictional forces and the pressure gradient force due to the horizontal density gradients. The extent to which the mean characteristics of the outflow are consistent with such a current can be tested using the simplified model of Lentz and Helfrich (2002). In their idealized two-layer model, the current is characterized by h, the depth of the foot of the front over the topographic slope, W, the total width of the front, and L_R, the deformation radius, which is also a measure of width of the front beyond the foot, in the offshore direction (Fig. 11). Given the transport of the flow, Q, the Coriolis parameter, f, the density difference between the

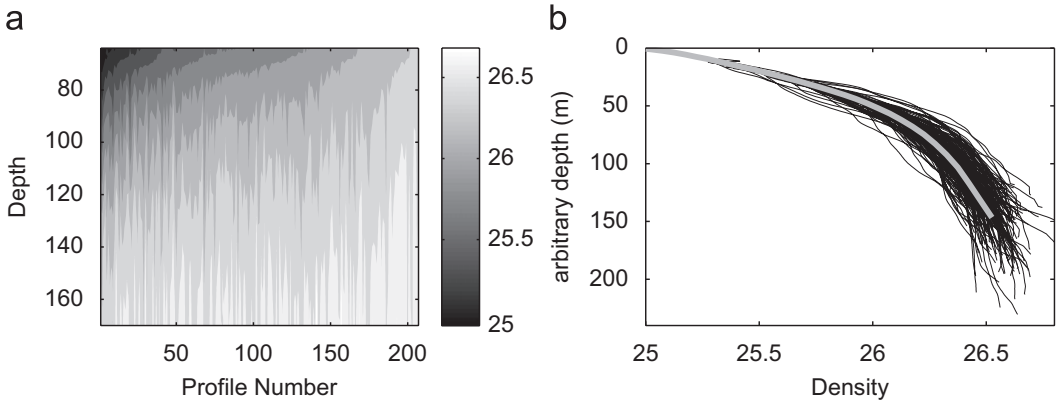

Fig. 9. (a) MMP profiles from August to March sorted as a function of the density at 60 m. (b) Reconstructed mean profile (gray) overlaid on the individual profiles (see text).

Author's personal copy

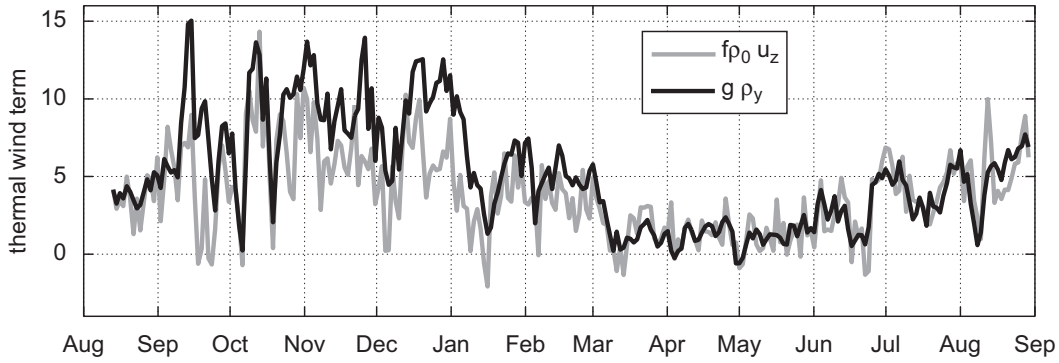

Fig. 10. Time evolution of the vertical shear in the along-strait flow direction and of the horizontal density gradient at 60 m at mooring B (units are $\times 10^{-4}$ kg/(m^3 s^2)).

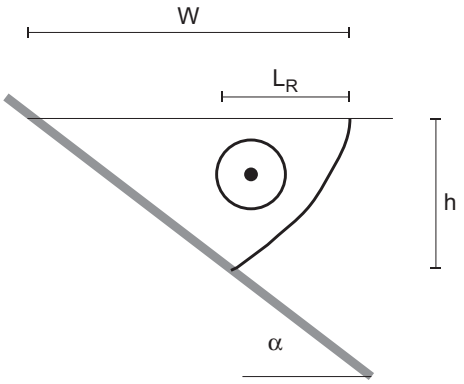

Fig. 11. Schematic of the structure of a buoyant, gravity current over sloping topography (redrawn from Lentz and Helfrich, 2002).

two layers which, in turn, defines the reduced gravity, g', and a topographic slope, α, the theory predicts that

$$h = \left(\frac{2Qf}{g'}\right)^{1/2} \quad \text{and} \quad W = \frac{h}{\alpha} + \frac{\sqrt{g'h}}{f}.$$

In the expression for the width, the first term represents the width of the front up to the foot while the second term, the deformation radius, gives a measure of the isopycnal slope.

Typical parameters for the Hudson Strait outflow are $Q \sim 1.1$ Sv (see following section), $f \sim 1.3 \times 10^{-4}$ s^{-1}, a density anomaly of 1 kg/m^3, which yields a reduced gravity g' of 0.01 m/s^2, and $\alpha = 0.01$ (300 m over 30 km). Given these, the model predicts a thickness of 170 m and a width of 27 km. The latter is considerably larger than the 7–9 km deformation radius that characterizes the outflow. Overall, the thickness and width are reasonable if one defines the buoyant fluid as that with density lighter than $\sigma_t \sim 26.4$—the density that separates the "fresh waters" from the denser waters of the HBS. On the other hand, the theory fails to predict the observed isopycnal slope by roughly an order of magnitude (as obtained from both the mooring data and the hydrographic data). This discrepancy is likely due to the two-layer assumption, which forces the sloping layer interface to be confined offshore of the foot and limited to a deformation radius. In a stratified outflow, one expects the isopycnals to be inclined across the entire width of the sloping topography.

5.3. Variability in the flow field

As observed in Section 4, the outflow tends to be faster when the freshest waters transit past the mooring on both seasonal and weekly time scales (Figs. 4, 5, 7 and 8). While causality cannot be assessed from time series alone, it is instructive to ask to what extent accelerations/decelerations of the flow are associated with density/salinity variations. To understand what relation one would expect between the two, we can build on the idealized two-layer system described above. Unlike the original model, however, we allow the density of the light layer (layer 1) to vary in time to be consistent with observations at the moorings. Note that characterizing the density of the fresh water (the buoyant layer) using a single density (at any given time) is consistent with the fact that across-strait variations are much smaller than temporal variations (Figs. 4 and 5). Similarly, we do not expect the deep and central waters of Hudson Strait to vary relative to the buoyant outflow since these are not affected by the seasonal fresh water input. This assumption is supported by moored data from the central portion of the strait, which shows little density variation in either the upper or the deep layers, for the period mid-September to mid-November 1982, even while considerable change is occurring in the outflowing waters (data made available by K. Drinkwater, 2004).

Given this idealized representation of the outflow and assuming semi-geostrophy in the along-strait direction, the baroclinic velocity can be written as

$$u_{bcl}(t) = u_1(t) - u_2(t) = \frac{gH}{f\rho_0 L}(\rho_2 - \rho_1(t)),$$

where H and L are the vertical and lateral scales of the flow and layer 2 represents the dense layer. According to this model, then, we expect the baroclinic flow to co-vary with the density of the upper layer.

Following this argument, we decompose the demeaned along-strait velocity into a portion that co-varies with the density variations of the upper part of the water column

Author's personal copy

plus a residual:

$$u'(t) = u_{\mathrm{bcl}}(y,z,t) + u_{\mathrm{R}}(y,z,t)$$
$$= \beta(z)\frac{gH}{f\rho_0 L}\delta\rho(y,z=40,t) + u_{\mathrm{R}}(y,z,t).$$

For simplicity, given the high coherence of density variations with depth at all moorings, we use the density at 40 m as representative of the density variations of the upper layer. The function $\beta(z)$ is an amplitude function that is allowed to vary with depth and can be determined via least square fits. The quantities H and L are chosen to fit our observations ($H = 300$ m and $L = 40$ km) though, effectively, their values affect only the amplitude of $\beta(z)$ and not the correlation. This decomposition is applied to the velocity records from moorings C and B, at all depths, and to the reconstructed 60 m velocity at A (see Appendix B). The baroclinic and residual velocities at 40 m at B are representative of the baroclinic and residual velocities obtained at all three moorings (Fig. 12a). While not assumed *a priori*, and consistent with geostrophy, the residual flow is essentially barotropic at both B and C where we have data throughout the water column.

We find that, in general, the lower frequency (weekly to seasonal) variability in the along-strait velocity is synchronous with density variations while the higher frequency variability is not (Fig. 12a). The amplitude function, $\beta(z)$, decreases linearly with depth (Fig. 12b), consistent with the decreasing baroclinicity and associated lateral density gradients as seen in the hydrographic data (Fig. 2). The fraction of variance that can be attributed to the baroclinic versus the residual, barotropic, flow decreases with depth, from about 60% in the surface layer at B to close to zero at 100 m, and onshore, from about 70% at 60 m at A to about 35% at 60 m at C (Fig. 12c). The residual, barotropic flow contains the larger amplitude, higher frequency variability and has no visible seasonal cycle. It is significantly correlated at all three moorings with correlations between A and B of 0.84 and of 0.63 between C and B.

To summarize, we find that approximately 50% of the velocity variance of the upper layers in the outflow is synchronous with density variations that occur on weekly to seasonal scales. Higher frequency and amplitude fluctuations at the three moorings are associated with a mostly barotropic flow which is observed across the array. The origin of these fluctuations is presently unclear. In a preliminary analysis of the impact of local winds, we found that only about 10% of this residual, barotropic flow can be correlated with local wind (derived from the GEM model reanalysis). Other possibilities include remote atmospheric forcing over Hudson Bay (e.g., Wright et al., 1987; Middleton and Wright, 1991).

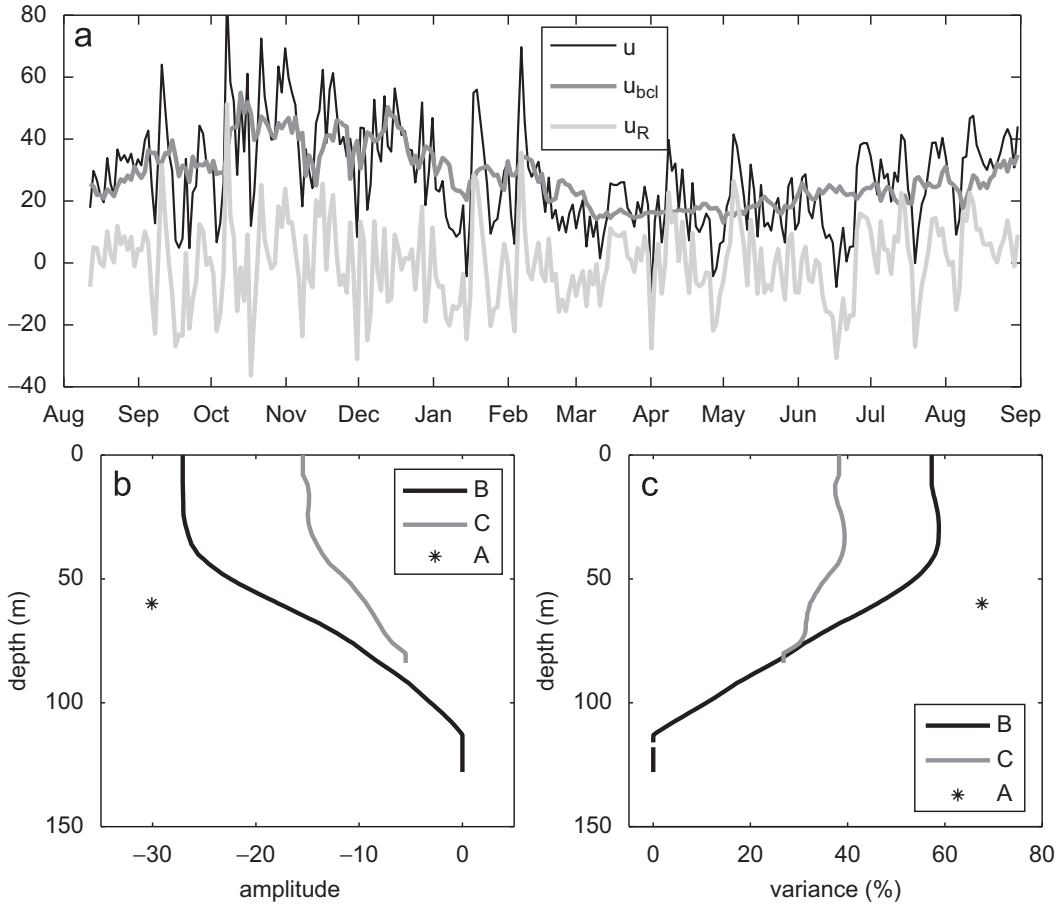

Fig. 12. (a) Decomposition of the along-strait flow at 40 m at B (black) into a baroclinic component, which co-varies with density (dark gray), and a residual (light gray). The baroclinic component is shifted by an amount equal to the average mean flow over the record to differentiate the two, (b) amplitude function $\beta(z)$ (see text) as a function of depth for C, B and at 60 m at A, (c) fraction of the variance explained by the baroclinic flow for the same data as in (b) as a function of depth.

Author's personal copy

6. Transport estimates

As discussed above, Hudson Strait is an important gateway for the exchange of properties, freshwater in particular, between the arctic and subarctic regions (Dickson et al., 2007), yet, prior to this field program, our knowledge of what transits through the strait was extremely limited. In terms of direct observations, the only previous estimate of volume transport is described by Drinkwater (1988) from four moorings deployed for 2 months only in 1982 in a section roughly 150 km to the east of ours. Two of these were located in the outflow, one in the inflow, and one in the middle of the strait; they carried approximately two current meters each (one at 30 m and one at 200 or 100 m). From these data, Drinkwater estimated an outflow of 0.93 ± 0.23 Sv and an inflow of 0.82 ± 0.24 Sv. Fresh water transport estimates for the strait have been made for the net transport only (outflow minus inflow) and are based on the assumption that the net export must roughly balance the riverine input plus the input from Fury and Hecla Strait yielding a net fresh water export of approximately 40 mSv (relative to a salinity of 34.8), equivalent to a fresh water input of approximately 900 km^3/yr (Straneo and Saucier, 2008).

The mooring data described here, thus, provide us with the opportunity to estimate the annual transports and their variability for the first time. As always is the case with oceanic transports, the estimates contain a degree of uncertainty. First, as is typical of moored data, interpolation and extrapolation must be applied to fill data gaps and cover depths with no data. Second, the moorings occupied only about half of the outflow and the transport estimate for the full outflow can only be made by making several assumptions about its structure. To differentiate between the uncertainties introduced by the various assumptions made, we break the transport estimate up in two steps. First, we present estimates for the annual mean and time-varying volume, heat and fresh water transports observed across the moored array (and extrapolated to the coast, 7 km from our first mooring). Next, we use both the summer hydrographic data, information from the 1982 and 1986 mooring deployments, and our measurements to infer the width of the outflow and estimate the volume and fresh water transport across the entire outflow. We note that because the ULS did not record sea-ice draft, we will be presenting estimates for the *liquid* portion of the fresh water, volume and heat transports only.

The freshwater transport is here defined as the transport of the anomaly with respect to a reference salinity (i.e., the spatial integral of $u(S_{ref}-S)/S_{ref}$, where u is the along-strait velocity). Because of the sensitivity of the freshwater transport to the chosen reference salinity we present two estimates. One uses a reference salinity of 34.8, the mean salinity of the Arctic Ocean, and typically used in quantifying the freshwater budget of the Arctic region (e.g., Dickson et al., 2007). The transport estimated using this reference salinity enables us to compare Hudson Strait's contribution to that of the other fresh water pathways into the North Atlantic. The second estimate uses a reference salinity of 33. This is our best estimate of the salinity of the inflowing waters as obtained from the summer section (Fig. 2) since there are no year-long records of properties on the northern side of the strait. This value is also consistent with observations from the outflow from Davis Strait (Cuny et al., 2005), which likely feeds the inflowing current into Hudson Strait. We expect the transport estimate using the inflowing salinity as a reference value to essentially reflect the net inputs into the HBS from rivers and Fury and Hecla Strait (since, by definition, the inflowing transport is zero).

Like salinity, heat transport is only meaningful with respect to a reference temperature. In Hudson Strait, the mean temperature of the inflowing waters is approximately 0 °C (again from the summer hydrographic data); thus we use this as our reference temperature. For comparison, the value typically chosen to compute heat transport in the Arctic ocean is −0.1 °C (Dickson et al., 2007) and hence not significantly different from the value employed here. Heat transport is then defined as the spatial integral across the array of $u\rho_0 c_w(\theta-\theta_{ref})$ where ρ_0 is the reference density (1027 kg/m^3), c_w the specific heat capacity (3900 J/(kg K)) and θ the potential temperature.

6.1. Transports from the coast to mooring A

The transport estimates presented below were obtained using the 34-h low-pass filtered data. For consistency, we verified that calculating the transport after filtering the data for tides did not introduce a bias. We did this at B and C (both at 40 and 60 m) and found that the difference between filtering the transport (calculated from the hourly data) or calculating the transport from the filtered data was under 1% in all cases.

6.1.1. Interpolation/extrapolation of the property and velocity data

At moorings B and C, temperature recorders covered the water column from 40 to 140 m and 36 to 100 m, respectively. These records were linearly extrapolated to 10 m below the surface, beyond which a mixed layer is assumed. At B, a 10 m bottom mixed layer is assumed. Salinity records, on the other hand, are only available at 40 (35) m and 60 (55) m at B (C). These are extended to the top and bottom through linear interpolation and extrapolation and by assuming a 10 m (20 m) surface (bottom) mixed layer. When utilizing this method at C, we find that the density at the bottom is always less than 26.4, suggesting that the waters transiting at C, and onshore, are the fresh waters of the HBS at all times of the year. At B, if we linearly extrapolate to 130 m we obtain densities that are unrealistically large (denser than 26.7, which is the maximum density observed in the strait). To correct for this, we assume that waters denser than 26.4 have a fixed stratification $N \sim 0.006\,s^{-1}$, in agreement with both the summer hydrographic data and the analysis of the profiler data shown in Fig. 9. Assuming this stratification is due to salinity alone, it is equivalent to a salinity gradient of 0.0047 per meter. Once this method is applied, the maximum density observed at B is 26.7, consistent

Author's personal copy

with both the hydrographic data and the profiler data at A. The data gridding at A is described in detail in Appendix A. As for B and C, a 10 m surface and 20 m bottom mixed layers are assumed.

For velocity, the ADCPs at B and C provide records between 10 and 20 m from the surface to 20 m from the bottom. These gaps are filled by assuming uniform velocity over the surface layer and extrapolating the observed shear to fill the bottom layer. The surface extrapolation is supported by the observation that the shear in the flow tends to decrease towards the surface layer (see, for example, the mean profiles of Fig. 6). At depth, we note that horizontal density gradients are non-zero (hence we expect the flow to be sheared) and, unlike the center of the strait, we do not observe deep mixed layers in the property field. Following this extrapolation the bottom velocity at C (100 m) is 7.6 cm/s while that at B (150 m) is 2 cm/s. We note, however, that our transport estimates are not overly sensitive to how these two data gaps are filled. Indeed, our extrapolation yields a minimum transport estimate at each mooring and, if we had done the opposite (i.e., assumed a sheared flow at the surface and a mixed layer at depth), the maximum transport estimate would have been only about 1–2% larger, and hence negligible compared to some of the larger uncertainties in our estimate.

The long-range ADCP at A failed after 21 days of operation, leaving us with no direct velocity measurements at this mooring for most of the year. Using the tilt record from the ULS (at 60 m) at A, however, we were able to reconstruct the along-strait velocity at 60 m based on an empirically derived relationship between the mooring tilt and the observed along-strait speed (see Appendix B). Using the derived velocity at 60 m, the velocity at A throughout the entire water column is then reconstructed using two different methods, an empirical and a dynamic one. The former relies on the assumption that the velocity at depth (130 m) at A is directly proportional to that at the nearby mooring B. The latter makes use of the gridded density data and geostrophy to derive the shear at A. The two methods are described in detail in Appendix B. Here, we compare transport estimates using both velocities. Velocity, temperature and salinity are extrapolated to the coast, 7 km from C, by assuming that properties at the coast are identical to those at C. If anything, we expect this assumption to slightly underestimate both the volume and freshwater transports.

6.1.2. *Transport estimates*

Before presenting the transport estimates across the sampled portion, it is useful to consider the depth and time averaged velocity, salinity and temperature (transport-weighted) at each of the three mooring locations (Table 1). Errors of the mean shown are calculated by assuming a decorrelation timescale of 5 days, which means that of the 258 measurements (of the 34-h low-passed filtered, subsampled timeseries) only 73 are independent. This decorrelation time scale is an upper estimate obtained by evaluating the zero crossing of the autocorrelation functions of the velocity (and properties) at all three moorings having removed the seasonal cycle.

Table 1
Transport-weighted mean velocity, temperature and salinity at the three moorings

	U (cm/s)	T (°C)	S
A: empirical	18.4 ± 1.1	-0.75 ± 0.13	31.93 ± 0.11
A: dynamical	18.7 ± 1.4	-0.91 ± 0.25	31.59 ± 0.64
B	17.2 ± 1.2	-0.62 ± 0.16	31.47 ± 0.26
C	17.7 ± 1.4	-0.54 ± 0.19	31.19 ± 0.11

The two estimates for A are obtained using the two different reconstructed velocity fields (see Appendix B).

Thus, these errors simply reflect the uncertainty of the mean due to the high-frequency fluctuations. These mean values confirm that the freshest and warmest waters transit close to the coast. They also show, however, that the averaged velocity across the array is relative uniform and hence that the gradients in temperature and salinity are mostly due to property gradients and not velocity variations. Finally, we note that the two reconstructed velocities yield very similar estimates for the mean fields at A.

Next, we compute the volume, heat and fresh water transports by gridding the interpolated/extrapolated fields and computing the time-varying fluxes (Fig. 13). Like velocity, the volume transport is characterized by a weak seasonal variability but larger amplitude and higher frequency fluctuations. For fresh water, the seasonal variability has a larger amplitude than the higher frequency variability that is due to the high frequency velocity fluctuations. Fresh water transport peaks between November and December (when the lowest salinities are observed) and approximately 70–80% of the freshwater transport occurs between August and mid-February. For heat, given the narrow window when temperatures are different from freezing, the transport bears a strong resemblance to the seasonal surface heating/cooling cycle of the region and, in particular, to the summer heating that occurs over the narrow window of open waters (July–November over much of the region).

Estimates for the mean annual transports between the coast and mooring A are given in Table 2. The uncertainties given reflect, as above, the significance of the mean with respect to the high-frequency fluctuations once the seasonal signal has been removed from the 34-h low-passed filtered transport time series. The decorrelation timescale was found to be on the order of 4 days (for all transports), thus giving us 86 independent measurements out of the 258 that cover the entire year (at a 34-h time interval). Note that we found that the estimates of all transports did not vary significantly whether we used the empirically or the dynamically reconstructed velocity fields at A: in all cases the difference was within the uncertainty given. Thus, in Table 2, we present only the estimates using the dynamic velocity, since we believe this to be the most accurate.

Next, we compare the extent to which the transports obtained by first annually averaging the property and the velocity fields differ from those calculated by first calculating the flux and then averaging (the volume

Author's personal copy

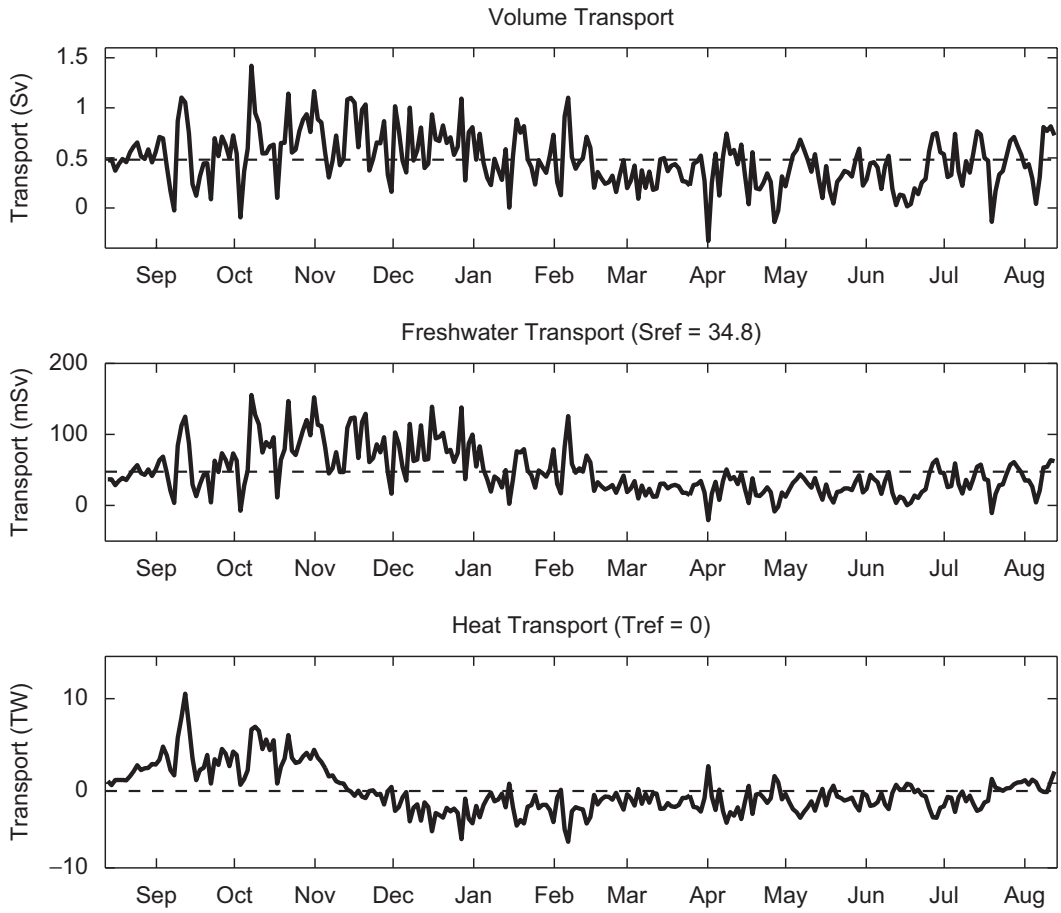

Fig. 13. Volume, heat and freshwater transports from the east coast to mooring A (21 km offshore) as a function of time. The dashed horizontal line represents the mean estimate.

Table 2
Volume, freshwater and heat transports estimated: (1) from the coast to A from the time varying records (column 1), (2) from the coast to A from the annual means (column 2), (3) across the full outflow assuming a width of 45–55 km (column 3)

Transport	Coast to A	Coast to A from annual mean	Full 45–55 km
Volume (Sv)	0.48 ± 0.03	0.48	1.0–1.2
Freshwater (mSv)—34.8	47.6 ± 3.5	44.8	78.4–88.6
Freshwater (mSv)—33	23.9 ± 2.3	20.9	27.1–28.0
Heat (TW)	-0.93 ± 0.27	−1.28	–

Units are Sverdrups ($\times 10^6$ m^3/s) for volume, milli-Sverdrups for freshwater relative to two different salinities, and TeraWatts ($\times 10^{12}$ J/s) for heat.

transport does not change). We find that changes in the fresh water transports are limited to 6% (12%) for the transport referenced to 34.8 (33) and of the order of 25% for the heat transport. In general, these errors are within the uncertainties due to the high-frequency fluctuations. A discussion of the estimated transports is postponed to the next section.

6.2. Transports across the entire outflow

We estimate the transport across the entire outflow by extrapolating the mean (annually averaged, spatially variable) velocity and property field towards the middle of the strait to a reasonable estimate of the outflow's width. We extrapolate the mean fields, and not the temporally varying records, since we have little information on the temporal variability mid-strait (of velocity in particular). The width of the outflow is diagnosed by examining both the existing moored data from the 1982 and 1986 arrays (data provided by K. Drinkwater, BIO/IMR) and from the hydrographic data collected in summer 2005.

The 1982 array consisted of four moorings, deployed from mid-September to mid-November, two of which were located in the outflow, one mid-strait (60 km from the southern shore) and one in the inflow. These were located approximately 150 km downstream of our mooring array, but, given the relatively uniform along-strait bathymetry, we do not expect the flow structure to differ

Author's personal copy

significantly between the two sections. This is confirmed by Drinkwater (1988), who reports that the width of the boundary current along the southern slope appears to be fairly constant throughout the strait. Data collected from the 1982 array is restricted to a 2-month period, yet from our year-long observations, we expect the mean over these 2 months to be representative of the annual mean. Drinkwater (1988) found that the velocities at depths of 30 and 200 m mid-strait were not significantly different from zero, suggesting that the edge of the outflow is less than (or equal to) 60 km. The moorings located along the southern coast, furthermore, recorded mean, along-strait flows of 30 and 7 cm/s at (30 m depth) at locations that were 10 and 40 km from the coast, respectively. Assuming a linear across-strait decay rate this suggests that the outflow width is approximately 48 km.

A second mooring array across the *same* section occupied by our array was deployed in 1986–1987 for a total of 11 months. Because of substantial instrument failure, these data have not been published but have been provided to us by K. Drinkwater (BIO/IMR). Of the four current meters, located across the outflow, that recorded data two were located roughly at the same position as B, i.e., 14 km from the coast, at depths of 30 and 100 m. Two more current meters were located further offshore over the 240 m isobath, 25 km from the coast (i.e., 4 km from mooring A of our array) at 40 and 200 m. The along-strait flow observed in the surface layer was of 30 and 22 cm/s at the onshore and offshore moorings, respectively, suggesting that the maximum outflow occurs onshore of 25 km from the coast. This is an important finding since we found maximum mean outflow at A, which is 21 km offshore. If we assume the same outflow characteristics in 1986–1987 as in 2004–2005, we can thus assume that the maximum outflow speed roughly occurs at A. Using the 1986–1987 upper current meter data, and assuming a linear decay rate, we expect the flow to be zero roughly 55 km offshore. Lastly, the mean flow at the offshore (25 km) mooring of the 1986–1987 array at 200 m was 3 ± 1 cm/s, which suggests that the flow at this location is mostly baroclinic with a weak barotropic component.

Finally, the summer hydrographic section shows isopycnals that flatten approximately 50 km offshore of the Quebec shore suggesting that the width of the baroclinic portion of the flow is thus contained onshore of the 50 km mark (Fig. 2). From these three data sets, collected at different times, we therefore infer that the mean flow, along the southern shore of the strait, tends to zero between 45 and 55 km offshore—an uncertainty that will be included in the transport estimate below.

The annually averaged mean salinity section, across the outflow, is reconstructed by combining the mean salinity from the moored array (0–21 km offshore) with the summer hydrographic data from 40 to 55 km. Our assumption is that in this offshore region the seasonal salinity variations are small such that the summer profiles are representative of mean conditions. It is supported by the fact that the fresh water (the largest source of seasonal variability) is trapped onshore and has limited impact mid-strait. It is also supported by the moored, mid-strait measurements collected in 1982 which showed limited variability (relative to the onshore moorings). A comparison of the reconstructed mean salinity with the hydrographic data collected in August 2005 is at least qualitatively supportive of the reconstruction (Fig. 14a). For velocity, it is assumed that the velocity offshore (at 55 km) is zero throughout the entire water column and the velocity from the moored array is interpolated to this zero-velocity line (Fig. 14b). For consistency, we compare the derived velocity with the geostrophic velocity one would expect given the reconstructed salinity field (temperature is assumed at freezing point—for simplicity—since it has little impact on the density) (Fig. 14b). The good agreement between the reconstructed velocity field and the geostrophic flow is again at least qualitatively supportive of our reconstruction. Finally, we do not attempt to reconstruct a temperature field since it is not as well behaved (or as dynamically significant) as salinity and overall we have little to compare it to.

The volume and fresh water transports estimated from the reconstructed means are given in Table 2. Because of the uncertainty on the width of the outflow, the transport is estimated as a range derived by assuming that the velocity is zero at either 45 or 55 km offshore. Both the volume and fresh water transports (relative to 34.8) roughly double with respect to those estimated across the array. This reflects the fact that a sizable volume flux (with salinities lower than 34.8) occurs offshore of mooring A. The fresh water transport with respect to a reference salinity of 33 across the full outflow, on the other hand, does not differ greatly from that observed across the array. This is because the waters flowing offshore have salinities close to 33 and hence do not contribute to the fresh water transport. The sensitivity of our estimates to the outflow width are evaluated by considering the cumulative volume and fresh water transports as a function of the distance offshore (Fig. 14c and d). For all cases, the transport has attained 90% or more of its maximum value by 40 km offshore—the distance where isopycnals begin to flatten. Thus, overall the dependence on the width estimate is relatively low provided it is assumed to be greater than or equal to 40 km.

6.3. Uncertainties in the transport estimates

The transport estimates presented here have relied on a series of assumptions that have led to data interpolation and extrapolation to fill data gaps. For the transport estimates between the coast and A, these mainly involved spatial interpolation between observations and extrapolation to the coast. Sensitivity studies indicated that for both velocity and properties the results were not overly sensitive to how we filled the bottom layers where we had no data. This is also true for velocity in the surface 10–20 m layer which the ADCP did not cover. Thus, uncertainties due to these extrapolations are estimated to be smaller than 5–10%. It is less clear, on the other hand, how large an uncertainty is due to extrapolation of salinity into the upper 35–50 m where we have no data. While we believe we have made the best guess at what the vertical

Author's personal copy

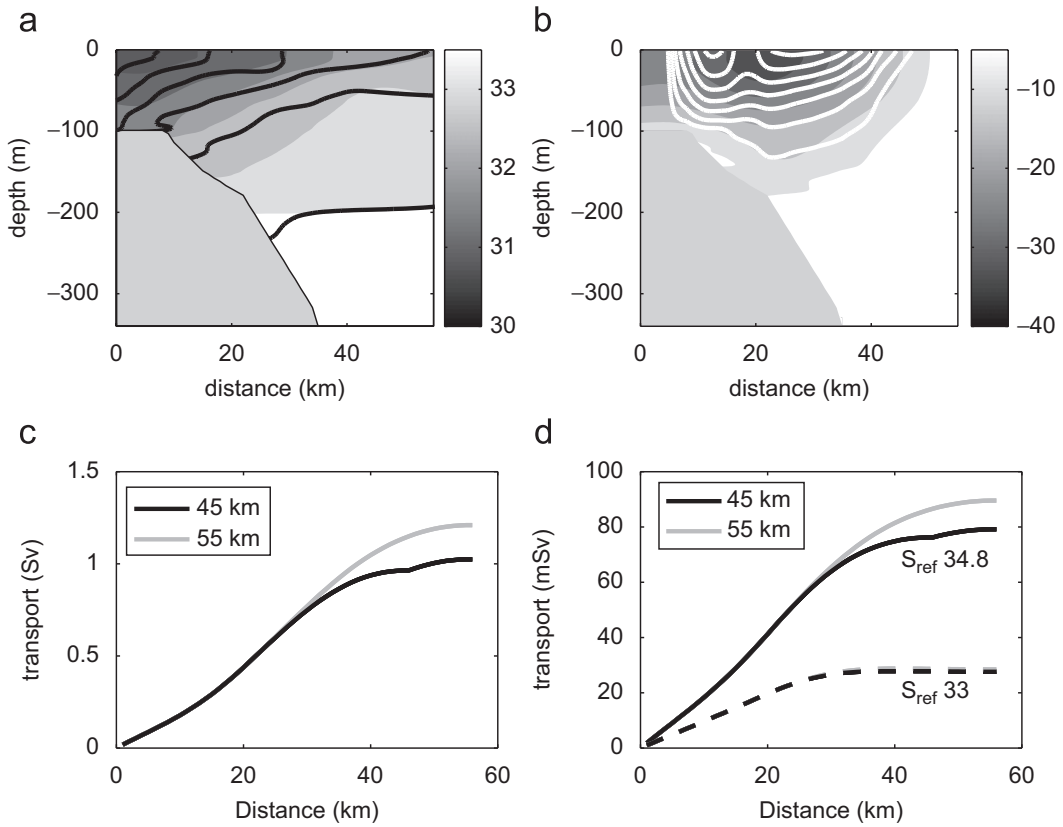

Fig. 14. (a) Reconstructed mean salinity; overlaid are the same salinity contours (dashed lines) from the hydrographic section of August 2005; (b) reconstructed mean velocity; overlaid are the geostrophic velocity contours (assuming zero velocity at the bottom, dashed white—same contour interval) from the reconstructed mean salinity (see text); (c) cumulative volume transport as a function of distance from coast; (d) same as (c) but for freshwater transport.

property structure might be, the lack of data does not allow us to explicitly quantify this uncertainty. From the data we have, however, it appears that the temporal variability in the property fields is much greater than the spatial variability which suggests that this upper layer extrapolation is not a source of major uncertainty.

Similarly, we do not believe that the extrapolation to the coast—assuming flat isopycnals and the same velocity profile as at C—is a major source of uncertainty. Both the hydrographic data and the knowledge that the distance between the coast and C is on the order of a deformation radius support our hypothesis. If anything, our extrapolation to the coast is likely to slightly underestimate both the volume and fresh water transports. Similarly, the variability in the fields yields an uncertainty of the mean estimate that is on the order of 10% (Table 2).

Greater uncertainties are introduced, on the other hand, in extrapolating the transport estimates across the full width of the outflow. First, for fresh water, we are assuming that the transport estimated from the mean fields is similar to that obtained from the annually averaged field. When we do this for the transport estimate from the coast to A, we find that the results differ by less than 15%. Second, our full width transports rely on our estimate of the width of the outflow. The fact that we obtained comparable estimates for the outflow width from a variety of sources (1982 and 1986 mooring data, and hydrographic data) plus the fact that the transport is not overly sensitive to the actual width we chose (as shown in Fig. 14) suggest that the dependency on the width itself is under 10%. Finally, even once we defined the width, we had to make assumptions on the structure of both the velocity and property fields in the unsampled part of the flow. For the velocity, we imposed a linear decay in the across-stream direction. For salinity, we assumed that conditions offshore of 40 km, in the central portion of the strait, were similar to those observed in our summer hydrographic section. These two assumptions are likely the largest source of uncertainty for the transport estimates and it is difficult to assess its degree. The fact that the geostrophic velocity estimated from the mean density (salinity) field has the same shape as that reconstructed, however, is indicative that our assumptions are at least consistent with the observed dynamical structure of the outflow. We assess the sensitivity of our assumptions by estimating the range given an outflow width of 45 or 55 km—if we consider the range indicative of the uncertainty, then it is 10–15% for the volume and fresh water transport (relative to 34.8).

To summarize, the analysis presented here provides an estimate of fresh water and volume (and partially of heat) transports in the Hudson Strait outflow. Where possible we have estimated the uncertainties due to the fluctuations of the flow and properties and, overall, we do not believe these to be the dominant source of uncertainty for these estimates. On the other hand, it is more problematic

Author's personal copy

to assess how large an uncertainty is introduced by the lateral (mostly towards the center of the strait) and the surface layer extrapolations we had to make to fill in areas where we have no data. These extrapolations were carried out by utilizing all available information and, in our opinion, are quite robust. Nonetheless, the present estimates still likely suffer from an uncertainty of the order of 10–20%.

7. Summary and discussion

Hudson Strait is the principal opening for the extensive HBS, a large subarctic/arctic estuarine basin that seasonally undergoes a complete cryogenic cycle. The HBS receives a large riverine input, which, combined with the inflow of Arctic Ocean water via Fury and Hecla Strait, makes it a substantial contributor to the fresh water budget of the subpolar North Atlantic. Circulation in Hudson Strait is two-way: towards the HBS along its northern coast (the inflow) and towards the Labrador Sea along its southern coast (the outflow). While it has been recognized for some time that the outflow from Hudson Strait has a large impact on the properties and ecosystem along the Labrador Shelf (and on the downstream northeastern seaboard) and is an important pathway for fresh water, the absence of year-round observations has greatly hindered our understanding of the role it plays in shaping the structure and variability of the Labrador Current it feeds. This study describes the first year-long survey of the outflow from Hudson Strait via a mooring array located roughly mid-strait. The moorings, deployed in the summer 2004 and retrieved in the summer 2005, measured temperature, conductivity and velocity both at discrete depths and along profiles. These measurements have allowed us not only to quantify the volume and fresh water transports in the outflow, but also to describe its properties and its variability.

The Hudson Strait outflow carries fresh, cold waters from the HBS, along the coast of Quebec, towards the Labrador Sea. The freshest waters are exported between June and March with peak fresh periods from mid-October to mid-December. This seasonal variability is consistent with the strongly seasonal fresh water input due to rivers and sea-ice melt. The flow has the structure of a buoyant boundary current in semi-geostrophic balance and is stretched across the sloping topography with a mean width of approximately 45–50 km. The velocity variability is dominated by the strong tides (mostly the semi-diurnal) with flows on the order of 1 m/s and a tidal range that exceeds 8 m. The subtidal variability in the flow, on the other hand, is primarily due to high frequency (daily to several days), mostly barotropic fluctuations, which occur simultaneously across the entire array. These are not associated with fluctuations in the density fields and are likely due to both local and remote atmospheric forcing. On weekly to seasonal time scales, velocity intensifications are associated with the freshening of the outflow. The across-strait velocities have zero mean, when vertically integrated, but indicate that a net downwelling occurs at the Quebec coast that is consistent with the predominantly along-strait winds.

The outflowing water masses can be distinguished into two classes. The fresher waters ($S<33$) are highly stratified and primarily exported between June and March. These are the waters that have been freshened by the strongly seasonal riverine input and sea-ice melt. Their characteristic uniform stratification is indicative of strong mixing likely due, in part, to the large tides. The more saline ($S>33$) and less stratified waters are exported beneath the fresh waters, during the fresh outflow period, and throughout much of the water column between March and June.

The volume and fresh water transported by the outflow are estimated to be 1–1.2 Sv and 78–88 mSv (27–28 mSv) relative to a salinity of 34.8 (33), respectively. Note that the fresh water transport estimate is for the liquid portion only and that, even if not taken into account here, the export of sea-ice may contribute roughly another 6 mSv (Saucier et al., 2004). The volume transport is of the same order of magnitude as an earlier estimate based on 2 months of current meter measurements collected in 1982. If we compare these numbers to the estimated volume and fresh water (relative to 34.8) transports of the Labrador Current, 7.5 Sv and 180 mSv, respectively (Loder et al., 1998), our results suggest that *approximately 15% of the volume and 50% of the fresh water carried by the Labrador Current is due to the Hudson Strait outflow.* This is a striking new result, which suggests that we need to rethink the source waters for the Labrador Current and, in general, the fresh water pathways into the subpolar North Atlantic. It indicates that the role of Hudson Strait has been previously overlooked because of the absence of direct measurements from the strait.

We note that the large fresh water export observed in the outflow from Hudson Strait (relative to 34.8) is *not* inconsistent with the existing estimates of the *net* fresh water export from the strait (~40 mSv, i.e., approximately half; Dickson et al., 2007; Straneo and Saucier, 2008; Drinkwater, 1988). The first is an estimate of what flows out, while the last is an estimate of the difference between the inflow and outflow in the strait. Explicitly this means that the inflow is supplying approximately 44 mSv of fresh water to the HBS. If we assume that the volume transport of the inflow is approximately 1 Sv (the HBS is mostly an enclosed basin; therefore the net volume transport through Hudson Strait must be ~0.1 Sv, Straneo and Saucier, 2008); this, in turn, suggests an inflow salinity of approximately 33. It is revealing to consider the fresh water transport estimate relative to 33 since its magnitude (~30 mSv) is roughly equal to the net fresh water inputs via rivers and Fury and Hecla Strait (especially considering the large interannual variability of the riverine input—Déry et al., 2005). This is what one would expect given an inflow with a mean salinity of approximately 33. A more extensive discussion of the volume and fresh water budgets for the HBS is presented in Straneo and Saucier (2008).

It is interesting, at this point, to speculate about the source waters for the inflow. Most likely these relatively fresh waters are those flowing out of Davis Strait and hence are Arctic Ocean waters on their way to the subpolar North Atlantic. This hypothesis is supported

Author's personal copy

by observations of the flow at the mouth of Hudson Strait (LeBlond et al., 1981) and by the observation that properties over the Labrador Shelf differ from those over the Baffin Bay shelf south of Davis Strait (Lazier, 1982; Sutcliffe et al., 1983; Drinkwater and Jones, 1987), which call into question the existence of a dominant direct route of the surface waters from Davis Strait to the Labrador shelf. (An alternative source of waters for the inflow into Hudson Strait could be the West Greenland recirculation (Loder et al., 1998; Cuny et al., 2002); however, this appears to follow the 3000 m isobath around the Labrador Sea and hence to transit far offshore of the mouth of Hudson Strait. Indeed, none of the drifters shown in Cuny et al. (2002) head into Hudson Strait.) Dynamically such a detour is expected since there are no direct topographic contours connecting the sill at Davis Strait (~600 m deep) with the Labrador Shelf. Given the estimated volume and freshwater (relative to 34.8) transports out of Davis Strait of 3.3–4.6 Sv and 120–150 mSv, respectively (from Cuny et al., 2005; Loder et al., 1998), it follows that approximately 25% of the volume and 35% of fresh water flowing south via Davis Strait heads deep into Hudson Strait, instead of merging directly into the Labrador Current. This is not a trivial re-routing for a number of reasons. First, Hudson Strait is a region of strong mixing, which will lead to a substantial modification of the water properties (e.g., the properties of the inflowing waters observed in the summer hydrographic section). Second, while it is still unclear how far the inflow penetrates into the HBS, the fact that these waters are observed mid-Hudson Strait suggests that they may be involved in the water mass transformation processes that occur within the HBS, including sea-ice formation and entrainment of both riverine and sea-ice melt water. Thus, the inflow's properties are likely to be even more transformed. Finally, this re-routing will add both a seasonal and potentially a multi-year delay to the propagation of anomalies from Davis Strait to the Labrador Current, depending on how far into the HBS the bulk of the inflow reaches.

Acknowledgments

The authors would like to thank the Department of Fisheries and Oceans, the captains and crews of the NGCC Pierre Radisson and NGCC DesGroseillers, and technicians Sylvain Cantin, Roger Pigeon, Rémi Desmarais, Simon Senneville, James Ryder, Dan Torres, Rick Krishfield and Scott Worrilow. Straneo would also like to thank R. Pickart, R. Beardsley, S. Lentz and K. Drinkwater for their advice in the planning of the field work and in the subsequent analysis. K. Drinkwater also kindly provided access to the 1982 and 1986 data. D. Torres helped in reconstructing the velocity field and T. McKee is responsible for several of the figures. Straneo acknowledges support from the Woods Hole Oceanographic Institution's Ocean and Climate Change Institute and the Comer Foundation, in particular, as well as support from NSF OCE-0629411. Support to FJS came from NSERC Research Grant and the Canadian Program on Energy Research and Development.

Appendix A. Gridding and filling of the temperature and salinity data at mooring A

Mooring A carried a variety of instruments that recorded temperature and salinity which worked successfully to varying degrees. The data were gridded onto a regular time/depth grid both for analysis purposes and for the transport calculation presented in Section 6. Prior to this, the analysis described was performed on gridded data without any data gap filling save for minimal vertical interpolation over several meters that separated the Microcat at depth from the bottom of the MMP profile, and from the top of the MMP profile to the base of the Arctic Winch. For the transport calculation, on the other hand, we had to fill in more conspicuous data gaps (due to both the MMP and Arctic Winch failure).

The gridded temperature and salinity data at mooring A contains data from the following instruments:

i. MMP profiles—from 60 to 165 m every 2 h for the first 6 months and then irregular (Fig. 5).
ii. Arctic Winch daily T and S profile from 58 m to an average of 55 m (and at times to the surface).
iii. Microcat T, S record every half hour at 170 m.

Data from the different instruments were combined into a time versus depth grid as follows. First, depth was defined as the depth from the mean sea-surface elevation (or equivalently as depth from the bottom). This avoids confusion due to the large variation in the sea-surface height (O(8 m)) and is straightforward for the fixed depth instruments, such as the Microcat. Data from profiling instruments, MMP and Arctic Winch, on the other hand, is collected as a function of pressure from the surface. These were converted into depth from the bottom measurements by removing the instantaneous sea-surface height anomaly (with respect to the annual mean). The anomaly is obtained from the high-resolution (20 s) pressure record at 58 m from the Upper Looking Sonar. It is noted here that the tilt in the mooring was very small, because of the 2000 lb buoyancy of the top float, and that the vertical excursion of the ULS due to tilting in the mooring was always less than 2 m. For all purposes of this study, this tilting is assumed negligible. The pressure record from the ULS, which ran out of power on 15 July 2005—45 days from the end of the deployment, was extended using pressure data from the Microcat at 40 m on mooring B. This is legitimate, given the high correlation in sea-surface height variability at all three moorings.

When the MMP was profiling every 2 h, the MMP profiles (ending at 165 m) were simply extended to 170 m via linear interpolation to the 2-h low-passed T, S records from the Microcat. This generated regularly gridded data from 60 to 170 m every 2 h until 7 March and irregularly time spaced data after this date. These data were then used to derive a daily gridded profile, centered on the time when the Arctic Winch profiled. The averaged daily profile was then extended to the winch profile via linear interpolation.

Author's personal copy

When the MMP was profiling irregularly, both the MMP and Microcat data are first averaged into daily bins. The MMP temperature and salinity profiles are then interpolated to the daily averaged Microcat T, S measurements at 170 m. The Arctic Winch record from 60 m provides daily T and S values. Any gaps in the Arctic Winch record are filled using linear regression from the Microcat at 60 m from the nearby mooring at B (the correlation, where data exists, is significant and with $r>0.8$). The combined MMP and Microcat profiles are then extended to the Arctic Winch data via linear interpolation where the profile extended to at least 80 m. The remaining data gaps are filled by assuming that profiles with similar T, S properties at 60 m are identical. This is consistent with the analysis presented in Section 5. Because temperature was effectively close to the freezing point, over the period when the MMP profiles are incomplete, this relation is essentially dominated by salinity. Thus, data interpolation methods are restricted to vertical interpolation. This is more realistic than any time-interpolation given the high-frequency variability of the filtered data. While there is no way of testing the validity of this gap filling method—a series of analyses conducted on the gridded time series yielded physically realistic results. For example, the correlation between the property data at B at 60 m and the observed data at A rapidly decreases beneath 80 m. This feature is also true in the reconstructed data set.

Appendix B. Reconstruction of the velocity field at mooring A

The ADCP at A, which measured velocity over the top 150 m, failed after 21 days. By using the available ADCP measurements, the tilt record from the Upward Looking Sonar (ULS), and the reconstructed density field, we were able to reconstruct the velocity at A for the entire mooring deployment. The method involves two distinct steps. First, the high-resolution tilt data from the top of mooring A (at 60 m), the available ADCP data and the velocity at the nearby mooring B (7 km away) are used to derive the along-strait flow at A at 60 m. Next, to reconstruct the velocity throughout the entire water column we use the derived flow at 60 m, together with the reconstructed density profiles and the dynamic features of the flow discussed in Section 5.

Step 1. Along-strait velocity at 60 m

Mooring A was designed to be very stiff, given the strong currents in the Strait, by using a 2000 lb buoyant sphere as the top float at 60 m. This sphere carried the ULS, which recorded the mooring's absolute tilt from deployment until 15 July. The tilt of the mooring reflects its drag to the currents, and it was straightforward to find an empirical relation between the absolute tilt and the speed at the mooring over the 21 days when the ADCP was functioning. Because we are unsure of how the mooring tilts (e.g., as a rod or flexing) we decided that this empirical relation was more appropriate than using a model for drag due to the mooring. (As for mooring B (Fig. 7) the flow field at A is dominated by the along-strait velocities; hence we assume that these are dominant throughout the entire record.) Thus, using the 21 day-ADCP record from A, we investigated the relationship between the tilt and the along-strait speed at various points of the water column and averaged over different depth intervals. While the tilt and the speed are significantly and highly correlated at all depths, the highest correlation ($r=0.87$) was found with the along-strait speed at 60 m (Fig. 15a). This is perhaps to be expected since this is the depth where the large buoyant sphere (1.5 m diameter) is located—thus offering a large drag higher up in the water column. A third-order polynomial was found to fit the data the best (higher order polynomials did not decrease the norm of the residuals) (Fig. 15a).

Using this empirical relation, we reconstructed the speed of the along-strait flow at 60 m until 15 July at hourly intervals. We note that at this point we know only the magnitude of the flow not its sign. We derived the sign by assuming that it was in the same direction as the along-strait component of the flow at B. Over the 21 days when we have data this was found to be consistently true.

Finally, the 11-month reconstructed record at A at 60 m was extended one more month using an empirical linear relation (Fig. 15b) between the along-strait velocity at B and that at A obtained from the 21-day ADCP record. The reconstructed along-strait flow at 60 m at A is compared to the observed 21-day record and to the low-passed flow field at B, at the same depth, in Fig. 15c. This shows the very high agreement with the initially observed record and also a high correlation between the two moorings—even at lower frequencies.

We note that given the high correlation between the flow at A and B observed during the period when the ADCP was working, we used this same empirical method to reconstruct the flow field at A, at 60 m, from B alone (without using the ULS tilt). In terms of the transport calculation, the two methods give effectively very similar results. Still, we feel that the first method, which employs an independent instrument located at A, is a better choice than utilizing the flow field at B.

Step 2. Vertical structure of the along-strait flow at A

We here present two independent approaches to reconstruct the vertical structure of the flow field at mooring A, given the velocity at 60 m. The first method is entirely empirical while the second makes use of geostrophy. The two resulting velocities are compared below.

The empirical method relies on the assumption that, at depth, the velocity at A is directly proportional to that observed at the nearby mooring (B) close to the bottom. Physically, we justify this on the finding that the baroclinic flow at depth is weak and that the flow is dominated by barotropic fluctuations, which are highly synchronous throughout the array. Explicitly we assume that the velocity at A at 130 m is linearly related (in time) with the velocity at B at the same depth. The best fit to the

Author's personal copy

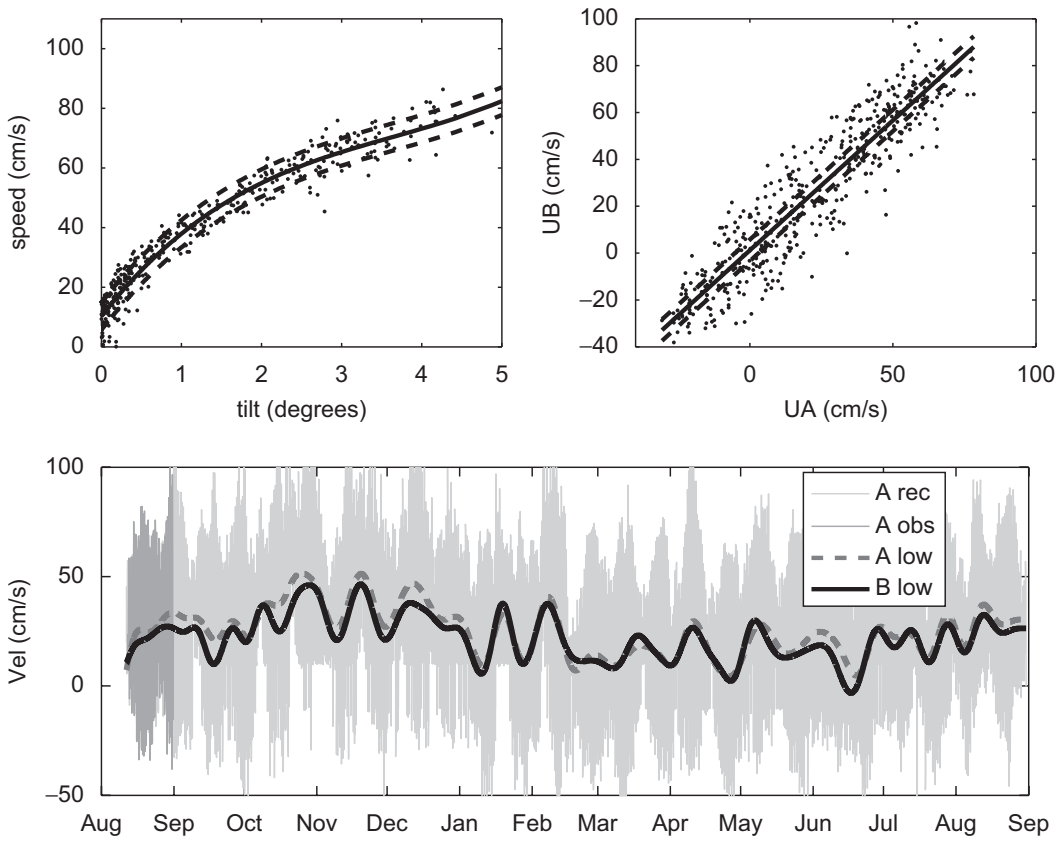

Fig. 15. Reconstruction of the along-strait flow at 60 m at A: (a) along-strait flow at A at 60 m (from the short ADCP record) versus tilt of the mooring. Also shown is the cubic fit with the 95% confidence intervals. (b) Relation between the along-strait velocities at 60 m at A and at B; the linear fit is superimposed. (c) Reconstructed flow field at 60 m at A. Overlaid are the short observed record from A, and the 2-week low-pass filtered flow for the observed record from B and the reconstructed field from A.

relation is obtained from the 21 days while the ADCP was working and yields a coefficient of 1.17 plus an offset of +3.2 cm/s. Given the velocities at A at 60 and 130 m, we linearly interpolate to obtain the velocity between these two depths and extrapolate further to 10 m from the surface and 20 m from the bottom. Mixed layers are assumed over these two layers.

An alternative dynamic method to reconstruct the along-strait velocity at A makes use of the assumption that the flow is in thermal wind balance. We assume that the across-strait density gradient at A is equal to that observed between B and A and thus can be obtained from the gridded density fields at both moorings. This assumption is supported by the uniform isopycnal slope, observed across the outflow, during the summer 2005 (Fig. 2) and, in general, by analysis of the profiler data at A. Given geostrophy, the horizontal density gradient and the velocity at 60 m, one can derive the velocity at A from 10 to 150 m. This velocity is subsequently extrapolated to 160 m, and 10 m (20 m) mixed layers at the top and bottom are assumed.

It is reassuring that these two different methods yield very similar results (Fig. 16). For example, the vertically and time-averaged flow using the empirical and dynamic method yields the similar estimates of 18.4 and 19.7 cm/s, respectively. We note that while the two methods are not totally independent (the velocity at 60 m is the same in both), their agreement reflects the generally well-behaved

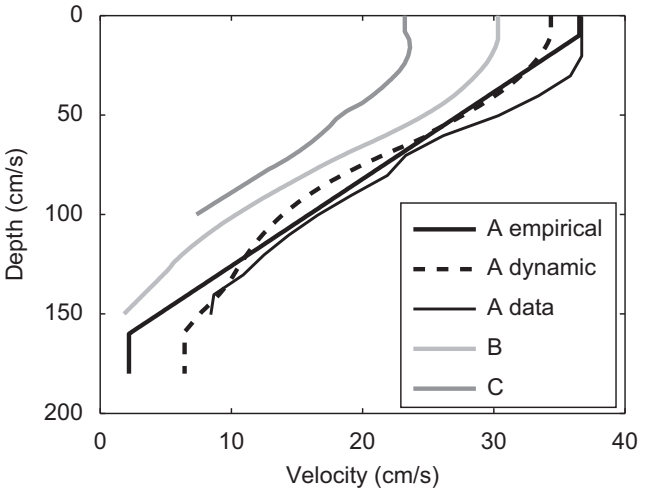

Fig. 16. Temporally averaged (over 1 year) along-strait velocity at A using the empirical and dynamic methods described in the text. Also shown are the yearly average velocities at B and C, and that observed during the 21 days of ADCP operation at A.

structure of the flow. The main difference between the two is that the dynamic method tends to concentrate the shear in the upper layers, where the fresh water is concentrated. This is consistent with the observation that the horizontal density gradients decay rapidly at depth. These two reconstructions are, furthermore, consistent if

Author's personal copy

compared to the mean velocity observed at A while the ADCP was running and, in terms of structure, with the mean profiles observed at B and C. The mean deep velocity observed at depth at A (2.2 cm/s for the empirical and 6.4 for the dynamic method) is consistent with the 3 cm/s observed during the 1986–1987 deployment of a current meter at 200 m at a mooring that was 5 km offshore of A (unpublished data provided by K. Drinkwater, BIO/IMR).

References

Chapman, D.C., Beardsley, R.C., 1989. On the origin of shelf water in the Middle Atlantic Bight. Journal of Physical Oceanography 19, 384–391.

Cuny, J., Rhines, P.B., Niiler, P., Bacon, S., 2002. Labrador Sea Boundary Currents and the fate of Irminger Water. Journal of Physical Oceanography 32, 627–647.

Cuny, J., Rhines, P.B., Kwok, R., 2005. Davis Strait volume, freshwater and heat fluxes. Deep-Sea Research I 52, 519–542.

Déry, S.J., Stieglitz, M., McKenna, E.C., Wood, E.F., 2005. Characteristics and trends of river discharge into Hudson, James, and Ungava bays, 1964–2000. Journal of Climate 18, 2540–2557.

Dickson, R., Dye, S., Karcher, M., Meincke, J., Rudels, B., Yashayaev, I., 2007. Current estimates of freshwater flux through arctic and subarctic seas. Progress in Oceanography 73, 210–230.

Drinkwater, K.F., 1986. Physical Oceanography of Hudson Bay and Ungava Bay. In: Martini, I. (Ed.), Canadian Inland Seas. Elsevier, Amsterdam, pp. 237–264.

Drinkwater, K.F., 1988. On the mean and tidal currents in Hudson Strait. Atmospheric-Oceans 26, 252–266.

Drinkwater, K.F., Harding, G.C., 2001. Effects of the Hudson Strait outflow on the biology of the Labrador Shelf. Canadian Journal of Fisheries and Aquatic Sciences 58 (1), 171–184.

Drinkwater, K.F., Jones, P., 1987. Density stratification, nutrient and chlorophyll distributions in the Hudson Strait region during summer and their relation to tidal mixing. Continental Shelf Research 7, 599–607.

Greene, C.H., Pershing, A., 2007. Climate drives sea change. Science 315, 1084–1085.

Ingram, R.G., Prinsenberg, S., 1998. Coastal oceanography of Hudson Bay and surrounding Eastern Canadian Arctic Waters. In: Robinson, A.R., Brink, K.N. (Eds.), The Sea, Vol. 11. The Global Coastal Ocean Regional Studies and Synthesis. Wiley, pp. 835–861.

Jones, E.P., Anderson, L.G., 1994. Northern Hudson Bay and Foxe Basin: water masses, circulation and productivity. Atmospheric-Oceans 32, 361–374.

Lazier, J.R.N., 1982. Seasonal variability of temperature and salinity of the Labrador Current. Journal of Marine Research 40 (Suppl.), 341–356.

Lazier, J.R.N., Hendry, R., Clarke, A., Yashayaev, I., Rhines, P., 2002. Convection and restratification in the Labrador Sea, 1990–2000. Deep-Sea Research I 49, 1819–1835.

LeBlond, P.H., Osborn, T.R., Hodgins, D.O., Goodman, R., Metge, M., 1981. Surface circulation in the western Labrador Sea. Deep-Sea Research 28A, 683–693.

Lentz, S.J., Helfrich, K.R., 2002. Buoyant gravity currents along a sloping bottom in a rotating fluid. Journal of Fluid Mechanics 464, 251–278.

Loder, J.W., Gawarkiewicz, G., Petrie, B., 1998. The coastal ocean of northeastern North America (Cape Hatteras to Hudson Strait). In: Robinson, A., Brink, K. (Eds.), The Sea: Ideas and Observations on Progress in the Study of the Seas. Vol. 11: The Global Coastal Ocean: Regional Studies and Syntheses. Wiley, Toronto, 1062pp.

Mertz, G., Narayanan, S., Helbig, J., 1993. The freshwater transport of the Labrador Current. Atmospheric-Oceans 31, 281–295.

Middleton, J.F., Wright, D.G., 1991. Coastal-trapped waves on the Labrador Shelf. Journal of Geophysical Research 96, 2599–2617.

Myers, R.A., Akenhead, R.A., Drinkwater, K.F., 1990. The influence of Hudson Bay runoff and sea-ice melt on the salinity of the inner Newfoundland shelf. Atmospheric-Oceans 28, 241–256.

Prinsenberg, S.J., 1988. Ice-cover and ice-ridge contributions to the freshwater contents of Hudson Bay and Foxe Basin. Arctic 41 (1), 6–11.

Prinsenberg, S.J., Loucks, R.H., Smith, R.E., Trites, R.W., 1987. Hudson Bay and Ungava Bay runoff cycles for the period 1963 to 1983. Canad. Tech. Rep. Hydrog. Ocean Sci. 92 (viii), 71.

Saucier, F.J., Senneville, S., Prinsenberg, S., Roy, F., Smith, G., Gachon, P., Caya, D., Laprise, R., 2004. Modelling the sea ice-ocean seasonal cycle in Hudson Bay, Foxe Basin and Hudson Strait, Canada. Climate Dynamics 23, 303–326.

Schmidt, S., Send, U., 2007. Origin and composition of Seasonal Labrador Sea Freshwater. Journal of Physical Oceanography 37, 1445–1454.

Serreze, M.C., Barrett, A.P., Slater, A.G., Woodgate, R.A., Aagaard, K., Lammers, R.B., Steele, M., Moritz, R., Meredith, M., Lee, C.M., 2006. The large-scale freshwater cycle of the Arctic. Journal of Geophysical Research 111.

Straneo, F., 2006. Heat and freshwater transport through the central Labrador Sea. Journal of Physical Oceanography 36, 606–628.

Straneo, F., Saucier, F., 2008. The arctic–sub arctic exchange through Hudson Strait. In: Dickson, R.R., Meincke, J., Rhines, P. (Eds.), Arctic–Subarctic Ocean Fluxes: Defining the Role of the Northern Seas in Climate. Springer, New York, p. 740.

Sutcliffe Jr., W.H., Loucks, R.H., Drinkwater, K.F., Coote, A.R., 1983. Nutrient flux onto the Labrador Shelf from Hudson Strait and its biological consequences. Canadian Journal of Fisheries and Aquatic Sciences 40, 1692–1701.

Wright, D.G., Greenberg, D.A., Majaess, F., 1987. The influence of bays on adjusted sea-level over adjacent shelves with application to the Labrador Shelf. Journal of Geophysical Research 92, 14610–14620.